Article:

Patacci, M, Haughton, PDW and McCaffrey, WD (2015) Flow behaviour of ponded turbidity currents. Journal of Sedimentary Research, 85 (8). 885 - 902. ISSN 1527-1404

https://doi.org/10.2110/jsr.2015.59

FLOW BEHAVIOR OF PONDED TURBIDITY CURRENTS

MARCO PATACCI[1,2], PETER D. W. HAUGHTON[1], AND WILLIAM D. MCCAFFREY[2]

[1]UCD School of Geological Sciences and UCD Earth Institute, University College Dublin, Belfield, Dublin 4, Ireland

[2]Turbidites Research Group, School of Earth and Environment, University of Leeds, Leeds LS2 9JT, UK

Keywords: flow ponding; flow mechanics; internal waves; turbidites; onlap

ABSTRACT

Sea-floor topography can constrict, deflect, or reflect turbidity currents resulting in a range of distinctive deposits. Where flows rebound off slopes and a suspension cloud collects in an enclosed basin, ponded or contained turbidites are deposited. Ponded turbidites have been widely recognized in slope mini-basins and on small, structurally confined basin floors in strike-slip and foreland-basin settings. They can have a variable internal structure the significance of which remains poorly understood in terms of flow behavior. New experiments demonstrate that the ponding process can comprise up to four phases: 1) cloud establishment, 2) inflation, 3) steady-state maintenance, and 4) collapse. The experiments explored the behavior of sustained turbidity currents draining into small basins and show that the ponded suspensions that form are characterized by an important internal interface; this divides a lower outbound-moving layer from an upper return layer. The basal layer evolves to constant concentration and grain size, whereas the upper layer is graded (concentration and grain size decrease upward). During the cloud inflation stage, the concentration and velocity profiles of the ponded suspension evolve, and this phase can dominate the resulting deposit. Outbound internal waves can travel along the interface between the outbound and return layers and impinge against the confining slope, and their amplitude is highest when the density contrast between layers is greatest, e.g., when the input flows are thin and dense. The experiments show that flow reversals can arise in several ways (initial rebound, episodic collapse of the wedge of fluid above the counter slope, "grounding" of the internal velocity interface) and that despite steady

input, velocities decay and the deposit grades upwards. Internal waves emanate from the input point, i.e., do not form as reflections off the counter slope. The internal grain-size interface within the suspension may dictate textural trends in sands onlapping the confining slopes. Where flows are partially ponded, internal waves can generate pulsing overspill to basins down dip.

INTRODUCTION

Turbidity currents are gravity-driven "turbid" flows of water and sediment that transfer sand from the continental shelf to the deep ocean floor (Kneller and Buckee, 2000 and references therein). Flows can be of variable concentration (low- or high-density) and although noncohesive, they can evolve to become flows with cohesive behavior (e.g., hybrid flows of Haughton et al., 2009). Many turbidity currents travel down slope and out across open basin floors, where they decelerate leaving a bed with a predictable geometry and internal structure (e.g., Bouma, 1962; Lowe, 1982; Mutti, 1992). However, turbidity currents can meet counter or lateral slopes, particularly where they enter structurally-controlled or salt-controlled "mini-basins" (e.g., Kneller et al., 1991; Haughton, 1994; Winker, 1996; Sinclair, 2000; Al Ja'Aidi et el., 2004; Amy et al., 2004; Jobe et al., 2012). When a current encounters topography at a scale the same as or greater than the flow thickness, the flow can be deflected, reflected, or constricted, depending on the geometry of the slope and the angle of incidence of the current (Bursik and Woods, 2000; Alexander and Morris, 1994) as shown in Figure 1A-C. These processes can be generically referred to as "flow confinement" (cf. Pickering and Hiscott, 1985). When the confining topography partially or totally traps the current, resulting in the establishment of a flat-topped suspension cloud, the term "flow ponding" is used (see Van Andel and Komar, 1969). This can occur if the flow is discharged into a topographic low or if it backs up behind a constriction such as a narrow outlet channel (e.g., Twichell et al., 2005).

The behavior of ponded turbidity currents depends on the relative volume and duration of the flow compared to the size and geometry of the basin. Figure 1D summarizes four end-member ponding styles, based on the duration of the flow (surge vs. sustained) and the capacity of the flow to escape the basin (partial vs. full ponding). It should be noted that for sustained flows the degree of ponding can change during the life of the flow (see below). Surge-like flows result in rapidly collapsing ponded suspensions which may travel and be reflected across the basin only once or twice. These flows can be partially or fully ponded depending on the ability of the confining slopes to contain the entire current. Sustained flows can lead to a larger number of scenarios (from full to partial ponding): (a) the entire flow is trapped within the deep topography; (b) some of the frontal part of the flow is able to slop out as a consequence of the initial run-up but subsequently the suspension becomes fully ponded; (c) the flow is unable to slop out initially but the ponded suspension then inflates so as to eventually overspill the lip, or (d) the suspension overspills continuously following the first reflection (this is also the case when the ponded suspension backs up behind a constricted outlet channel).

Ponding results in the establishment of a sediment-bearing suspension cloud thicker than the original flow. The top of this sediment cloud is a subhorizontal, turbulence-free, detrainment interface (Lamb et al., 2004; Toniolo et al., 2006a and 2006b). The initial level of the interface is determined by the reflection behavior (scale of the bore), which is related to the thickness of the flow (Muck and Underwood, 1990) and the geometry of the counter slope.

In the case of a sustained-input flow, the ponding process can be divided into two main phases. The first is an unsteady “inflation” build-up phase during which the characteristics of the suspension cloud (height, velocity, and concentration structure) change coherently through time. This is followed by a quasi-steady phase when the same parameters are steady when averaged over a certain period. The build-up phase begins with the first reflection of the flow and the generation of an upstream-moving bore, and continues well after the establishment of the ponded suspension cloud and its subhorizontal upper interface.

Flow confinement (reflection, deflection, or constriction) and flow ponding of turbidity currents can lead to distinctive “confined” and “ponded” turbidites. Such deposits have been described from a number of ancient and modern basins (e.g., Pickering and Hiscott, 1985; Haughton, 1994; Kneller and McCaffrey, 1999; Muzzi Magalhaes and Tinterri, 2010; Remacha et al., 2005; Smith, 2004 and references therein), and a variety of bed types and characteristic features have been identified (Fig. 2), although the link between deposit structure and original flow behavior remains poorly understood.

Confined and ponded turbidites are economically important as they can host significant hydrocarbon reservoirs (e.g., Gulf of Mexico; see discoveries reported by Holman and Robertson, 1994, and Mahaffie, 1994), as they often comprise thick clean sandstone units which onlap muddy slopes that can provide a lateral seal (McCaffrey and Kneller, 2001; Bakke et al., 2013). Therefore, it is important to understand how the interaction of turbidity currents with topography can dictate changes in texture and thickness in the sands deposited.

Early flume experiments on confined turbidity currents focused on surge flows reflected or deflected against frontal (Pantin and Leeder, 1987; Muck and Underwood, 1990; Edwards et al., 1994) and lateral or oblique confining slopes (Amy et al., 2004; Kneller et al., 1991). These experiments described mainly the visible structures of the flow, including run-up height and the formation of bores and solitons, but they gave limited insight into the internal behavior of the current. Experiments by Lamb et al. (2004) and Toniolo et al. (2006a, 2006b) investigated flow geometry and concentration trends in fully and partially ponded sustained turbidity currents carrying a monodisperse grain-size distribution. Sequeiros et al. (2009) investigated mixed saline and sediment-bearing sustained turbidity currents meeting an obstacle and reported vertical profiles of streamwise velocity indicating a complex circulation pattern in the ponded wedge of fluid. However, the wide range of confined and ponded turbidite bed types is not explained by the current models, and many aspects of the flow behavior of a ponded turbidity current remain poorly understood.

This paper provides new insights into the behavior of sustained ponded suspension clouds, focussing on: a) 3D velocity structure, b) turbulence intensity, c) flow behavior during the build-up phase, and

d) trends in concentration and grain size for flows carrying a polydisperse grain-size distribution. The newly described flow structures have implications for deposits, particularly in onlap situations and thus for turbiditic stratigraphic traps. The link between flow behavior and the experimental deposit is discussed, leading to a better understanding of ponded turbidites in outcrop and in the subsurface.

EXPERIMENTAL SETUP AND PROCEDURE

Thirty-one experimental runs were undertaken at the Sorby Environmental Fluid Dynamics Laboratory (University of Leeds). Of these a subset of ten, representing a wide range of input conditions, are presented here. A number of experimental basins of various lengths and degrees of confinement were used. Table 1 and Figure 3A and B summarize the flow input parameters and the tank geometry for the runs considered in this paper. The experimental tank was filled to a depth of 80 cm with tap water and was nested within a larger water-filled flume tank. Water exchange between the two was possible at the free surface level on one side of the experimental tank and – in series L runs – above the lip of the confining slope.

Gravity flows were produced by mixing tap water and industrial glass beads (Vaquashene) with a narrow grain-size distribution and a median of ~ 40 µm (Fig. 3C). All input flows had a nominal concentration of 3% by volume. Fluid was prepared in a 2 m^3 mixing tank and was pumped either directly to the discharge system (Series G runs) or into a loop feeding a 70 liter head tank from where it drained by gravity into the discharge system (Series L runs). Fluid discharge was kept steady for 10 minutes to generate steady, noncohesive gravity flows that were fully turbulent (calculated Reynold numbers of the body of the generated currents varied between 10,000 and 30,000).

In Series G experiments, fluid was discharged into the experimental tank through a two-pipe system. Fluid was pumped into an inner vertical pipe, sealed at the end, from where it moved into a larger surrounding pipe through a number of 8 mm holes in the sidewalls. This mechanism was designed to prevent jet flow and to suppress mixing in order to generate thin and dense turbidity currents. At the end of the large pipe, a bend resting on the tank floor and facing down the tank allowed fluid release. In Series L experiments, fluid was discharged into the experimental tank through a single vertical pipe with a right-angle bend facing the back wall and positioned 10 cm away from it. The pipe was located at the top of a one-meter-long inlet slope dipping 10 degrees. This system was designed to produce strong mixing (i.e., making thick, low-density currents) while avoiding jet flow as the fluid reflects against the back wall and collapses gravitationally down the slope.

The generated flows can be approximated as two-dimensional “slot” flows (i.e., cross-flow gradients in flow structure are considered to be insignificant, apart from wall effects discussed below); lateral expansion of the flow occurred only at the point of discharge from the pipe. During fluid discharge an outlet pump located in the dump area of the outer tank was activated to remove enough fluid to ensure a constant water level. The dump area also helped in to minimize reflections off the back wall of the larger, containing flume tank in Series L experiments.

Velocity

An ultrasonic velocity profiler (UVP) was used to record the velocity field of the flow. UVP uses the information on Doppler shift frequency contained in an ultrasound signal emitted by a probe and echoed back by particles contained in the fluid. Each UVP probe measures the instantaneous flow velocity at 128 points along its axis (see Takeda, 1991, for a technical explanation of the methodology) extending 10 to 29 cm from the probe head in the configuration used. The orientation of two or three probes can be arranged in order that their measurement axes intersect. When three probes are arranged orthogonally to each other, it is possible to compute three-dimensional velocity vectors for their intersection point.

Twelve UVP probes were fixed into the side wall of the inner experimental tank, and one was fixed to a rigid support vertically 30.5 cm above the floor of the tank and oriented pointing vertically downwards, to allow non-intrusive measurement of three-dimensional velocity vectors along a vertical transect. The 3D velocity was recorded along a line orthogonal to the floor located between 2.5 and 20.5 cm above the floor and 12.1 cm from the side wall (Fig. 3D). This position slightly above the floor and almost in the middle of the tank was chosen to avoid the lower part of the current, where deposition takes place, and UVP measurements may cut out and to minimize any wall effects. Strong wall effects were measured within 5 cm of the walls during initial testing of the set-up.

Best et al., 2001 (and references therein) reviewed the principles of UVP methodology and its two key assumptions: 1) there is no slip velocity between fluid and suspended sediment, and 2) spatial change in flow density and therefore change in ultrasound velocity is less than the error limits in the methodology. The second assumption is perfectly valid at the concentration used (3% by volume) as reported by Best et al. (2001). The validity of the slip-velocity assumption is more difficult to assess because particle-turbulence interaction is not yet fully understood (see Leeder et al., 2005 for a review of current physical understanding). However, many authors have pointed out that small particles are more likely to follow fluid motion than larger grains (e.g., Owen, 1969; Hetsroni, 1989; Elchobashi, 1994). Best et al. (1997) used phase Doppler anemometry (PDA) to measure slip velocities for glass spheres in an open-channel flow recirculating at 57 cm/s. They showed that slip velocities for particles in the range 100-150 µm are ~ 2% of depth-averaged flow velocity and set a threshold of 88 µm to distinguish “fluid grains” (grains assumed to closely follow fluid motion) from “sediment grains”. In conclusion, the size of the particles in the current experiments (~ 40 µm) is small enough to infer that slip velocities would have been insignificant. The small ratio of the settling velocity of the particles (~ 0.14 cm/s according to Stokes’ Law) to the typical mean flow velocities (between 1 and 20 cm/s) reinforces this inference.

Calculation of RMS Velocity

“Root-mean-square” (RMS) velocity was calculated using the collected 3D velocity dataset according to the equation

$$v_{x\mathrm{RMS}} = \sqrt{\frac{1}{n} * \sum_{i=1}^{n} (v_{x,i} - v_x)^2}$$

where *n* is the number of samples, $v_{x,i}$ is the instantaneous velocity along the axis *x* at point *I*, and v_x is the average velocity along the *x* axis over the selected window.

The most significant issue when computing RMS velocity is the choice of a suitable time window. In the literature, very different choices are present (e.g., 7 to 37 s in Best et al., 2001; 1 s in Kneller et al., 1997; 1.87 s in Baas et al., 2005; 12 s in Buckee et al., 2001). The size of the window depends on the velocity sampling rate and the frequency rate in the dataset, and it is a compromise between preserving the detail of the small-scale turbulence fluctuations (for which a small window is better) and having a representative flow velocity average and a smooth resulting time series (for which a large window is better). In the present study the use of the UVP methodology allowed independent calculation of RMS velocity using a space window in addition to a more conventional time window. The former was possible thanks to each UVP probe measuring the instantaneous velocity for 128 points along the probe axis. The collected UVP dataset has a bin spacing of 1.48 mm and a sample frequency of ~ 2 Hz. A 2.4 cm space window (16 bins) and a 5 s time window (~ 10 bins) were chosen after initial testing as the best compromise. Note how the space window can be thought of as a more conventional time window considering the average flow velocity (e.g., average flow of 24 cm/s results in a 0.1 s time window and 2.4 cm/s in a 1 s time window). The space window allowed shorter-period fluctuations to be measured compared to the time window, which was more sensitive to longer-lived structures. Collected data show a very good degree of agreement between the two windows, strengthening confidence in the data interpretation.

Concentration and Grain Size

Sediment concentration and grain-size distribution of the suspension were measured from fluid samples collected during the runs through a siphoning system embedded into the side wall of the tank (“measuring localities” in Fig. 3A and B). Six pipes were inserted into holes drilled in the tank wall along a line orthogonal to the floor at the same distance from the inlet as the UVP probes but on the opposite side of the tank. In each pipe a constant flow of fluid (~ 230 ml/min) from the tank to a drain was achieved using a peristaltic pump. Flow velocity was set to ~ 20 cm/s. The value was chosen after preliminary testing as a good compromise between causing a small enough perturbation in the flow structure (for which a lower velocity is better) and avoiding any settling in the pipes and recovering enough sample (higher velocity better). Empty beakers were arranged on a sliding table, and at predefined time intervals (usually every 15 or 30 seconds) they were filled with the fluid issuing from the six siphoning pipes. The beakers were filled with ~ 30 ml in 8 seconds. Following the experiment, sediment concentration in the beakers was calculated by weighing the wet and dried content. For some of the runs, the dried sediment samples were wetted, disaggregated, and fed to a Malvern 2000 laser grain sizer to obtain measures of the grain-size distribution at different levels of the ponded suspension.

Velocity and Concentration Measuring Localities

Due to experimental constraints it was not possible to measure velocity and concentration at different localities during a single run. However, Runs L4 and L5 were designed to be repeats (same tank geometry and input flow conditions) in which only the measuring locations varied. L4 measuring arrays were in the flat part of the basin, while the L5 measuring locality was above the confining slope (see Fig. 3B). These twin runs are used through the paper to illustrate streamwise velocity gradients in the experimental tank.

Input flow discharge and concentration for these twin runs were monitored during their entire duration and very good similarity was achieved (1.91 l/s and 2.87% volume for L4 and 1.89 l/s and 2.88% volume for L5). On the other hand, input grain size could not be directly monitored, but evidence from the suspension cloud and the deposit suggests a D50 value of ~ 40 µm for L4 and ~ 35 µm for L5. This is assumed not to have a significant impact on the flow behavior and velocity profiles, but its impact on the concentration and grain size fields meant that streamwise gradients in concentration and grain size could not be inferred using this methodology.

Image Analysis of Video Recording

Video recordings taken through the side walls of the experimental tank were used to extract information on the internal structure of the flow. Quantitative calibration of the concentration values to extract concentration gradients was unsuccessful due to the nonlinear relationship between color and concentration and because of the difficulty of comparing areas far away from each other due to different light condition across the tank (different distance from light source and different angle of incidence of the light). However, on a tens-of-centimeters scale, the position of an arbitrary color threshold (representing a line of equal concentration) could be easily followed in a quantitative way and with good resolution. Such color thresholds in the flow were usually subhorizontal; therefore the height of a number of them at different vertical positions above the slope was a useful value to monitor. The height of a color threshold high in the flow can be used as a proxy for the position of the interface between clean water and dirty water, while the height of a color threshold in the ponded cloud can help to track the position of internal concentration isopycnals. This methodology also helps constrain the characteristics of the internal waves which displace such interfaces. Wave parameters such as phase velocity, frequency, and amplitude can be calculated from time series of the height of a selected color threshold.

Experimental Deposit

Deposit analysis was undertaken for a selected number of runs. After slow draining of the tank to minimize sliding, deposit samples were collected for a number of locations on the basin floor and above the confining slope. Laser particle sizing and SEM photography were used to characterize the deposit texture. Laser measurements are quicker but only allow vertically averaged measurements of the grain size. In contrast, SEM photography is lengthy (the sample has to be fixed, cut, and polished, and photographs have to be taken, stitched, and processed with image-analysis software), but this approach allows detailed vertical profiles of grain size to be measured.

EXPERIMENTAL RESULTS – FLOW BEHAVIOR

Reflection and First Basal Flow Reversal

When a turbidity current is released into the experimental tank, it travels along the basin until it meets the confining slope. After running up slope and reaching its maximum height the flow starts to collapse (see also Pantin and Leeder, 1987 and Edwards et al., 1994). The internal velocity structure of the current decelerating against the confinement is characterized by the development of a basal flow reversal on the confining slope (Figs. 4A and 5A). This is termed the "first basal flow reversal" to distinguish it from subsequent basal flow reversals seen in some experiments. The reversal travels toward the inlet, and although it tends to dissipate through time it can reach well into the flat part of the basin (Figs. 4B, C and 5B). On the slope, after the first reversal fades away it is initially succeeded by very low-velocity outbound flow (Fig. 4C) until faster outbound flow is re-established. In lower-velocity experiments (e.g., L6) the reversal may not occur; instead an area of very low outbound velocity is developed.

The generation of an upstream-migrating velocity reversal in the basal part of the current just above the confining slope is coupled to the occurrence of an upstream-migrating hump (bore) in the bulk flow. This thickening of the flow occurs as the outbound flow is forced to move upward as it approaches the area where the basal reversal occurs. This moving bore in surge-like experiments soon breaks into a series of solitons (Pantin and Leeder, 1987; Edwards et al., 1994). This is not observed in the present experiments, probably due to the sustained character of the input flow, leading to a longer-duration hump and also due to the short length of the tank, preventing the breaking to develop fully. Immediately after the passage of the bore, the thickness of the flow is increased by a factor of 1.5-2. As the hump reaches the inlet, the basin is filled by a sediment-bearing cloud which is thicker than the original turbidity current and has a sharp subhorizontal upper settling interface (Fig. 4D; Toniolo et al., 2006a, 2006b).

Velocity Structure

The ponded cloud during the inflation phase presents a 3D velocity structure with a number of distinctive features that are maintained through the entire duration of flow input. After the flow reversal fades and gives way to a newly established outbound flow, the horizontal streamwise component of the velocity within the ponded cloud becomes layered. An outbound basal layer is overlain by a return flow layer. A third thin upper outbound layer can also be present but is volumetrically less significant. The interface that separates the basal outbound layer from the upper return flow is here termed the "internal velocity interface" (Figs. 4D, 5E).

The vertical component of the velocity within the ponded cloud is also significantly affected by ponding. In an unconfined current such as L3 the average vertical velocity is close to zero (Fig. 6A). However, when a confining slope is added to the configuration (L4), with other boundary conditions and the measurement locality being the same, a significant upward-directed average vertical velocity is recorded (Fig. 6B). This upward velocity decreases toward the confining slope, as shown in Figure 6C, and it is expected to disappear completely higher up the slope.

The overall flow structure can be described as a large-scale circulation cell that carries sediment away from the input in the lower layer, transfers it upward in the downstream half of the basin, and returns it toward the input through the upper layer (Fig. 4D). The upward-directed component of the velocity in the flat part of the basin is interpreted as result of the deceleration of the outbound flow against the confining slope. Part of the momentum of the outbound flow, which is obstructed by collapsing flow above the confining slope, is "diverted" upward. This interpretation is supported by the similarity of this process with the upward shift of the outbound flow when meeting the first flow reversal (Fig. 4A, B). As sediment is continuously moved upward by this mechanism, this is interpreted to be the main pathway whereby sediment is delivered to the upper parts of the sediment-bearing cloud. It follows that when the basin extends in length to the point that this mechanism cannot operate (i.e., the outbound velocity is too low at the point of incidence with the slope for any part of the flow to become superelevated), turbidity-current ponding is not achieved and the flow behaves effectively as if unconfined.

Turbulence Distribution

The presence and role of turbulence in a ponded turbidity current has been questioned by Toniolo et al. (2006a, 2006b), who consider the flow to be passively collapsing following passage through a hydraulic jump on basin entry. Turbulence intensity can be evaluated using RMS velocity as proxy (Kneller et al., 1997; Buckee et al., 2001). The methodology and its limitations are described above.

RMS velocity values in a contained turbidity current are significant, though smaller than those recorded in a similar but unconfined flow. In ponded conditions, RMS velocity in the middle of the basin is ~ 75% of an unconfined flow and it decreases to ~ 50% above the confining slope (L4 and L5 compared to L3) as shown in Figure 6G-I. Higher values are usually recorded in the lower half of the flow, and this is consistent for ponded and unconfined flows, even though the increased flow thickness in case of ponding does not allow direct comparison of vertical velocities.

The turbulence intensity in the ponded suspension is thought to be dependent on the strength of the turbulence characterizing the inlet flow and also possibly by local generation of turbulence in the ponded basin, due to flow-substrate interaction or interaction between velocity layers. Flow collapse off the confining slope is also a likely mechanism for generation of turbulence. High turbulence is thought to promote a higher rate of cloud inflation because of lower sedimentation rate due to bed-load re-suspension and due to greater turbulent diffusion of sediment. However, a quantitative estimation of such effects has not been attempted as part of these experiments.

Concentration and Grain-Size Structure

The concentration and grain-size structure of the ponded suspension is also stratified. A basal flow layer with constant concentration and grain size is overlain by an upper fining-upward flow layer with a corresponding decrease in concentration. The surface separating the two layers is termed the "internal concentration interface" (Fig. 7). In those experiments for which appropriate data are available (run Ga) the position of the breaks in the gradient of concentration and grain size are seen to coincide. The relationship between the internal concentration interface and the internal velocity interface is hard to constrain due to the presence of internal waves (see below). However, it appears that they too at least crudely coincide (Fig. 7).

Internal Waves

Internal waves are oscillations that travel within the interior of a fluid and can propagate due to the stratified density structure of the medium (see Apel, 2002, for a review on the physics of internal waves). They characterize all the ponded suspensions generated, and video recordings show that they consistently travel along the internal density interface toward the confining slope (Fig. 8A, B). Smaller-amplitude internal waves can also be observed along the upper interface or within the graded upper layer.

Waves are manifested both in the vertical and the horizontal component of the velocity field, and they describe an orbital motion (Fig. 8D). The related velocity fluctuations extend through most of the suspension, not only at the interface position.

When the waves reach the confinement, either they spill over the lip or they dissipate on the slope. There is no evidence of the waves being reflected off the confining slope. When waves overspill the lip, they generate significant pulsing in the flows bypassing toward deeper bathymetry. Internal waves are symmetric; sometimes they can travel in packets of up to ten waves with the highest amplitude in the middle of the packet (e.g., observe time series for run L6 between 100 and 200 seconds in Fig. 8C). They develop as the suspension becomes stratified, and decay with time but do not entirely disappear. The amplitude and frequency of the internal waves appears to be related to the vertical density gradient within the suspension cloud. A sharp gradient results in higher-amplitude and higher-frequency internal waves (Fig. 8E).

The generation mechanism for the internal waves appears to be tied to the flow behavior of the turbidity current. Velocity pulses have been recorded within natural steady turbidity currents (e.g., Best et al., 2005); at the laboratory scale they appear to be related to the long-period turbulent structures, which can be observed as large-scale Kelvin-Helmholtz instabilities (which have similar durations of 5-20 seconds).

Velocity pulses within the turbidity current (e.g., Kneller et al., 1997) seem the most likely mechanism to generate internal waves, near the inlet, from where they travel toward the confining slope (cf. Tinterri, 2011, their Table 3). When the input flow enters the ponded suspension, the presence of the flow pulses disturbs both the upper settling interface and the internal concentration interface, with the second often being where the steepest concentration gradient is present, resulting in the most significant waves. Finally, it is speculated that reflection and constructive interference between internal waves could lead to increase in wave amplitude and energy. However, no wave-interference effects have been observed in the present experiments.

Basal Flow Reversals

Significant flow reversals can occur at the base of a ponded turbidity current or in the basal layer. Whereas negative local streamwise velocities can be present in the higher portion of any turbidity current as part of the Kelvin–Helmholtz instabilities, the occurrence of basal flow reversals in a turbidity current is related to the presence of confining topography.

According to their vertical location, duration, and vertical extent, basal flow reversals can be grouped into three types. Type A (“first basal flow reversal”) consists of high-velocity and highly turbulent return flow generated within the head of the current upon its reflection against the confinement. This has been described and interpreted above and can comprise one single reversal or a series of two or three in rapid succession (e.g., Fig. 9A). Type B (“downward-shift flow reversals”) usually lasts 2-10 seconds and consists of low-velocity flow structures occurring when the upper return layer shifts downward and reaches the floor (Figure 9B; see below for genetic mechanism). Finally, type C (“internal flow reversals”) includes isolated patches of return flow in the basal layer of the suspension cloud, which may or may not reach the floor. They can be the longest in duration (up to 30 seconds) and are generally of low velocity (Figure 9C).

Downward-shift flow reversals (type B) are commonplace in thin suspension clouds with significant internal waves. They are generated when the internal waves are able to push the internal interface between the basal outbound layer and the upper return layer down to floor level. On the other hand, internal reversals (type C) are generated in thick suspensions. In this scenario, a portion of the flow may collapse off the slope, causing the outbound flow either to entirely shift upward (resulting in an isolated basal reversal) or both upward and downward, leaving the return flow sandwiched between areas of outbound flow. The cross-flow extent of the reversals is difficult to establish, due to the slot nature of the experimental flows.

Inlet Flow and Ponded Suspension

The point where the inlet flow enters the ponded suspension is of particular interest. In the described experiments the inlet flow was always denser than the sediment cloud (and this seems to be a likely natural scenario), therefore it behaved as an underflow on entering the ponded suspension. However, other cases where the concentration of the inlet is similar to or smaller than that of the ponded cloud may lead to different flow behavior (e.g., interflows in lakes; see Best et al., 2005). It must be noted that in most of the present runs (except L7) the point where the fluid was released into the experimental tank became submerged by the ponded suspension during the experiment. In contrast, in natural examples the flow will always enter the ponded suspension from above, having been generated much higher up slope compared to the maximum height of the ponded cloud. However, because the inlet flow behaves as an underflow, this configuration appears not to affect flow behavior significantly and a hydraulic jump where the inlet flow enters the ponded suspension seems to be unimportant in governing the behavior of the sediment cloud (cf. Lamb et al., 2004; Toniolo et al., 2006a, 2006b). A hydraulic jump related to the slope break could occur in the underflow according to slope-break geometry and input conditions, but it could not be observed due to the opaque nature of the suspension cloud.

Flow Evolution during the Unsteady Build-Up Phase

After the ponded suspension is established (e.g., around two minutes from initiation of the current in L8), the unsteady build-up phase continues for a significant length of time (around eight minutes in L8). During this period, the ponded interface rises and the average concentration of the sediment cloud increases, as well as the concentration of the basal layer (Fig. 10). The rate of concentration increase in the overall cloud and in the basal layer declines asymptotically (closely following an exponential relationship) until a steady state is reached. The absolute value of the concentration reached in the basal layer depends on input flow discharge and concentration, while slope angle has no significant effect.

The unsteady phase is also characterized by a temporal decrease in the streamwise velocity component of the basal outbound flow. This drop is more important closer to the input (average velocity in L4 decreases by 50% during 10 minutes pumping time), while it is less significant on the confining slope, where slower velocities characterize the suspension from the beginning (see Fig. 6E, F). The change in flow velocity is interpreted as the result of the increase in concentration of the ponded cloud, leading to a reduction in density contrast between the inlet flow and the suspension it underflows.

Turbulence intensity and average grain size in the ponded cloud also decrease through time, as shown by Figure 6H, I and Figure 11. Decrease in turbulence intensity can be tied to the decrease in streamwise velocity. As a result of turbulence loss, the coarser grain sizes must be deposited in progressively more proximal locations through time, therefore average grain size in the cloud at a particular point must decrease.

EXPERIMENTAL RESULTS – DEPOSIT

Streamwise Grain-Size Trends in The Deposit

Bulk deposit samples allow streamwise deposit trends to be assessed (Fig. 12). Unconfined currents (e.g., L3) show no systematic change in grain size downstream (with the given input conditions and at the length scale of the tank), while ponded flows show fining up the confining slope, particularly when discharge is low and the degree of confinement high (e.g., L6). If discharge is high and confinement low, a very subtle fining trend can be recorded (e.g., L8). The coarsest deposit is measured on the lower part of the confining slope, whereas the values in the basin are usually slightly finer (Fig. 12).

The fining-upslope trend in the deposit is, perhaps, intuitive, and it appears to be linked to two factors: the decrease in near-floor velocity as the flow moves up the slope and the fining-upward vertical grain size gradient in the ponded cloud. Run L6 shows that grain size does not change much until the last 100 cm beyond the base of the slope (Fig. 12). This position corresponds to a height of ~ 20 cm (slope is tilted 10 degrees), which roughly corresponds to the measured position of the internal interface (see Fig. 7). The finer values recorded in the basin are likely caused by the accumulation of the very fine grains in suspension in the upper portion of the current (either by direct deposition at the end of the run or postdepositional remobilization of the very thin and fluid top layer).

Vertical Grain-Size Trends in The Deposit

Vertical profiles through the sampled deposit show a weak fining-upward grain-size trend through most of the bed, capped by a thin strongly fining-upward upper division (Fig. 13). The thick weakly fining-upward portion is deposited during the unsteady build-up phase, and the grain size trend can be predicted by observing the decrease in average grain size in the cloud during that phase (Fig. 11). In experiments where the suspension cloud is very thick, a significant part of this weakly fining-up portion of the deposit may be deposited by the collapse of the lower part of the ponded cloud. The upper thin cap is deposited after pumping stopped and most of the cloud collapsed; it represents the progressive deposition of the upper portions of the ponded sediment-bearing cloud (Fig. 13).

DISCUSSION

The experiments were targeted to investigate flow processes related to ponding of a fully turbulent and low-density, sustained turbidity current, to compare and contrast the results of the containment of surge-like currents (Pantin and Leeder, 1987; Muck and Underwood, 1990; Edwards et al., 1994) and to build on data and models provided by Lamb et al. (2004) and Toniolo et al. (2006a, 2006b).

The focus on the initial phases of the ponding process allows comparison and contrast with surge-like experiments (such as in Pantin and Leeder, 1987, and Edwards et al., 1994). In particular, in the experiments reported here the first reflection does not seem to produce a train of solitary waves. This is likely because of the sustained character of the input flow, leading to a longer-duration bore and to the short length of the tank, preventing the breaking to develop fully.

The condition through which a turbidity current can flow into a mini-basin and yet produce no outflow as concluded by Lamb et al. (2004) is confirmed by the these experiments. Similarly, the build-up of a ponded suspension characterized by a subhorizontal upper interface between dirty water and clean water, along which water detrainment takes place with virtually no turbulent mixing (Toniolo et al., 2006a, 2006b), is also observed.

The evolution of the ponded suspension under steady input condition consists of an unsteady phase, followed by a quasi-steady phase after equilibrium is reached. The unsteady build-up phase of the ponded process is significant in terms of duration and deposit. During this time, streamwise velocity, turbulence, and suspension grain size decay with time. The significance of this phase and its characterization are newly established results of these experiments.

The internal structure of a ponded turbidity current is layered. Two main layers can be recognized both in the velocity and in the concentration and grain-size structure. An outbound moving layer with constant concentration and grain size is overlain by a return layer characterized by a graded upward-decreasing concentration and grain size. The interface between the two layers, the “internal interface”, is a newly described feature.

In these experiments, the inlet flow entering the ponded suspension behaved as an underflow, and no hydraulic jump was observed at that location. Therefore, in this case a hydraulic jump cannot be a mechanism that feeds sediment into the ponded suspension, in contrast to the conclusions of Toniolo et al. (2006a, 2006b). The presence of a net upward-directed vertical velocity in the flat part of the basin and basin-scale circulation is suggested as an alternative mechanism. This has implications in terms of where the vertical mixing occurs: in the proposed model the maximum vertical mixing happens in the flat part of the basin not far from the confining slope rather than above the inlet slope.

Internal solitary waves are present in all of the generated ponded suspensions. Even though velocity fluctuations are likely to be characteristic of any turbidity current (e.g., Best et al., 2001) and could generate internal waves in unconfined flows, the presence of a sharp density interface within the ponded suspension appears to amplify the internal waves. Internal waves seem particularly important where they impinge and dissipate against the confining slope, because in this region the associated relative velocity fluctuations are highest.

For the first time turbulence in a sustained ponded turbidity current has been measured. The results show that significant turbulence is present in the ponded cloud, in particular at the base of the suspension; hence these results are in contrast to the theoretical conclusion from the model of

Toniolo et al. (2006a) that assumes turbulence in the ponded cloud to be very weak and unable to entrain sediment from the bed.

Gradients in concentration and grain size in the ponded cloud and grain-size deposit gradients are not directly accounted for in the work of Lamb et al. (2004) and Toniolo et al. (2006a, 2006b), in that they assume a mono-grain-size system for their interpretation. It should be noted that in their experiment they used a narrow but measurable grain-size range, and their data show – for example – deposit fining toward the confinement in case of strongly ponded currents (see average diameter decreasing from ~ 50 to ~ 40 µm for EXP1 in their Fig 12; Toniolo et al., 2006b); similar results were seen in the experiments presented here (e.g., see run L6; Fig. 12, this paper).

APPLICATION TO NATURAL EXAMPLES

The ponding experiments described (summarized in Figure 14) provide a useful framework for interpreting the deposits of suspension clouds in prototype confined settings. Here we focus on sheet-like, basin-centered sand-mud sheets produced by the high levels of containment that the experiments were designed to replicate. The experiments provide insight into the vertical sequence and types of sedimentary structures developed under these conditions, the origin of paleoflow variability, flow unsteadiness, and internal soft-sediment deformation that characterize many ponded turbidites (e.g., Pickering and Hiscott, 1985; Haughton, 1994; Remacha et al., 2005; Muzzi Magalhaes and Tinterri, 2010), as well as textural trends that might be anticipated, both vertically and laterally with respect to confining slopes (e.g., Kneller and McCaffrey, 1999; Amy et al., 2004; Davis et al., 2009; Patacci et al., 2014). Because the experiments involved slot flows, the results are probably most applicable in narrow basins such as those developed along strike-slip faults or controlled by growing folds (e.g., Smith, 2004). A better understanding of the pattern of internal circulation in enclosed basins that are more equant in plan form awaits new 3D basin experiments.

The 2D experiments demonstrate that beds emplaced by natural ponded flows may record up to four key stages: (1) runout before interaction with confining topography, followed by initial rebound and bore or soliton propagation; (2) inflation of a ponded suspension cloud (with or without overspill); (3) circulation of a quasi-steady ponded suspension; (4) deflation of cloud on waning of input and final settling of fines from a static cloud. The ratio of flow length to length of the confinement will dictate the extent to which stages 2, 3, and 4 are important, with long sustained flows and small receiving basins more likely to form circulating ponded suspensions as opposed to situations of flow rebound and rapid suspension collapse. Therefore, where ponded suspensions are formed and continue to be nourished by the inbound flow, the input characteristics and basin geometry can determine the relative importance of the different stages of the process preserved in the deposit. Longer flow durations, higher input concentrations, and shorter confinements will favor deposits that were mostly formed by the circulating suspension cloud (stages 2 and 3); shorter inflation periods and longer-range confinement will mean more of the deposit accumulates during the suspension collapse phase (stage 4).

The experiments reveal an important increase in concentration of the suspension cloud as it is progressively inflated by the inlet flow. The sandy components of some ponded turbidites are extensively laminated, and the concentration appears to have remained low throughout. However, others show an upward change from parallel-laminated and ripple-laminated basal sections to upper divisions of structureless or dewatered sandstone (e.g. Haughton, 2000). Beds of the latter type are consistent with increasing sediment fallout rate as the flow became ponded and the bed aggradation rate rose. Interestingly, beds with this character seem to be developed in small basins and sub-basins (generally kilometers rather than tens of kilometers across) such as Sorbas and Tabernas basins, SE Spain (Haughton, 1994) and the lower Castagnola system, Italy (Baruffini et al., 1994; Felletti, 2002). It would have been easier to sustain suspension clouds in these deep and relatively small basins. In contrast, reflected and ponded flows in larger foredeep basins (e.g., Marnoso Arenacea; see Muzzi Magalhaes and Tinterri, 2010; Hecho Group, Remacha et al., 2005) tend to be well laminated but often have wavy or sinusoidal bedforms developed in addition to current ripples. The sinusoidal bedforms resemble washed-out ripples at the transition from ripples to plane bed, formed on account of high near-bed sediment concentrations (Baas and de Koning, 1995) so these may also be indicative of higher sediment concentrations but not at the level that laminations are completely suppressed. Alternatively, these bedforms may record combined-flow processes associated with the interaction of internal waves with the near-bed unidirectional component of the ponded flow (Kneller et al., 1991; Tinterri and Magalhaes, 2011; Tinterri; 2011; see below).

The velocity structure of the ponded suspension clouds shows that they are dominated near the bed by an outbound underflow, but that this can be intermittently perturbed by periods of return flow. These return-flow episodes can relate to the initial rebound, to later instability in the wedge of fluid above the confining slope, or to depression of the internal concentration interface that allows the upper return layer to impinge on the bed. Velocities of the return flow are generally lower than the re-established outbound flow, and this means that deposits of the return flow could be reworked (at least in part) by the re-established outbound flow. In some cases where the initial flow is weak, even the initial rebound may not produce a reversal but instead a temporary deceleration of the outbound current. In all the cases examined, the periods of return flow at the bed are rather short-lived (and become less important away from the confining slope), and this is then hard to reconcile with natural deposits in which paleoflow indicators imply that return flow dominates the deposit (e.g., Tinterri and Muzzi Magalhaes, 2011; their Fig. 13). Beds exhibiting such reversals are more likely to form where the inbound flow is short-lived and the scale of the confining basin exceeds the typical flow length. Under these conditions, the flow can undergo complete reflection, and the sandy part of the deposit is then dominated by stage 1 (initial runout and rebound as a bore or train of solitary waves) with mud fallout from a static or gently sloshing cloud that was not inflated or sustained. The experiments do not capture the full range of possible interactions of the outbound flow with the confining slope, and it is possible other combinations of counter slope gradient and flow incidence angle can generate longer-lived flow reversals.

The underflow velocities beneath sustained suspension clouds are very unsteady, and the identification of a concentration interface as well as a detrainment interface in the suspension cloud helps account for this. Ponded turbidites are often characterized at least in part by repetitive alternations of internal divisions (“energy pulses” of Remacha et al., 2005) involving switching between massive or dewatered and laminated, laminated and convoluted, and parallel-laminated and ripple-laminated divisions (Kneller and McCaffrey, 1999; Felletti, 2002; Muzzi Magalhaes and Tinterri, 2010; see Fig. 2). Although pulsing or surging can occur under waning conditions in unconfined flows (e.g., Jobe et al., 2012) and is seen in the unconfined experiments (e.g., L3, Fig. 6D) in the present study, it is enhanced where the flow is ponded. Previous interpretations have stressed the role of reflected bores and waves running along the top of the suspension due to deflection and reflection of the currents (Kneller et al., 1991; Kneller et al., 1997; Haughton, 1994; Tinterri and Muzzi Magalhaes, 2011). However, at least in the experimental configurations studied here, strong internal waves propagate downstream from the inlet along the internal concentration interface and interact with the outbound flow layer beneath, forcing fluctuations in velocity, suspension fallout rate, and the propensity for liquefaction effects to occur and be expressed in the deposit (see Remacha et al., 2005; Muzzi Magalhaes and Tinterri, 2010). The implication is that not all internal waves propagate from the site of deflection or reflection. Tinterri (2011) attributes the presence of biconvex and rounded ripples with sinusoidal cross-lamination in ponded turbidites to pulsing combined flows in which there is an oscillatory component due to the presence of internal waves.

Once a ponded suspension becomes stratified, and if flow continues to plunge into and interact with the suspension from the inlet, it is likely that internal waves will run along the internal concentration interface. If the suspension inflates to overtop a downstream lip, the waves will generate an unsteady pulsed low-concentration overspill from the confined basin. A possible depositional expression of this process may the stacked ripple-laminated facies close to the downstream edge of the Titan mini-basin described by Jobe et al. (2012). A third mechanism leading to generation of internal waves relates to flow shutoff. In the experiments, rapid decay of the input sets up a series of decaying internal waves again triggered from the input point rather than the site of reflection. Ponded turbidites commonly have thin “sawtooth graded” layers of silt and sand beneath the mud cap or extensive pseudonodular silt units (Pickering and Hiscott, 1985; McCaffrey and Kneller, 2001; Remacha et al., 2005; Muzzi Magalhaes and Tinterri, 2010), and these may similarly be generated by unsteadiness in the flow caused by the shutdown of the input rather than by distal reflections. Once inbound flow decays, mud settles from suspension. There is often a sharp change from graded silty component of the bed (deposited from a disturbed suspension cloud undergoing resuspension of clay) to uniform mud, settling from a static suspension (Pickering and Hiscott, 1985).

Flow unsteadiness at longer time scales is expressed by a gradual decay of the underflow velocity and turbulence intensity as the suspension cloud inflates and the concentration rises. This is despite a constant input rate and concentration at the inlet. This is important because it means that for currents with a long inflation time, the bed will be weakly graded even though the input was sustained. The sandy parts of most ponded turbidites show normal grading, so this in itself is not an indication of surge as opposed sustained input. The experimental flows also show non-uniformity in the underflow, with lower outbound velocities and turbulent intensity on the lower counter slope relative to the basin floor for nominally similar flows, and with stronger streamwise non-uniformity than otherwise similar, but unconfined, currents. The lower outbound velocities on the slope are also prone to long-period stagnation (Fig. 6F) possibly due to underlying seiching set up by the initial rebound. This might explain why in a ponded basin the thinner beds on the edges of the ponded zone show internal structureless sand divisions (e.g., Haughton, 2000; Felletti, 2002). These may reflect a more rapid deceleration of the underflow during periods of stagnation within the onlap wedge combined with the overall rise in concentration as the suspension inflates.

The grain-size stratification in the suspension may impact the development of lateral trends in deposit character towards bed pinchouts against topography. Grain-size trends vertically in the suspension are uniform beneath the internal concentration interface but fine upwards above it.

Passive onlap of such a cloud will produce a lower-slope deposit with low rates of grain-size decline with a more rapid fall in grain size above the zone where the concentration interface impinges on the slope. Because the higher flow zone may be disturbed by internal waves, the deposit here may be strongly vacillitory (e.g., exhibiting the repetitions of Kneller and McCaffrey, 1999). Where the suspension partly overspills, grain-size gradients in the ponded deposit may be relatively muted (cf. experiment L6 vs. L8, Fig. 12).

CONCLUSIONS

The described experiments confirmed the occurrence of a number of phenomena described by previous authors:

a) Run up, reflection, and bore generation (Pantin and Leeder, 1987; Edwards et al., 1994);

b) Ponded suspension characterized by a subhorizontal dirty water-clean water upper interface (“ponded upper interface”) along which water detrainment takes place and with virtually no turbulent mixing (Lamb et al., 2004; Toniolo et al., 2006a and 2006b).

Newly identified aspects of the flow behavior of a sustained ponded turbidity currents and related deposit include:

1) The first reflection and the resulting bore can generate a significant basal velocity reversal, which travels into the basin;

2) Development of a two-layer circulation pattern (“internal velocity interface”) and average upward velocity component in the flat basin;

3) Significant turbulence characterizing the suspension cloud right up to the confining slope, albeit with a streamwise trend of decreasing mean turbulence;

4) Development of a two-layer velocity, concentration, and grain size structure, separated by an internal interface;

5) Internal waves related to flow pulsing and enhanced by confinement characterizing the suspension velocity structure;

6) In partially ponded conditions, internal waves result in flow surges downstream, which may be expressed in downstream deposits;

7) The inlet flow entering the ponded suspension behaves as an undercurrent: no hydraulic jump is present at this location;

8) Unsteady phase of suspension inflation controlled by input condition and characterized by: concentration build-up, velocity decrease, turbulence intensity decrease, average suspension grain size decrease;

9) Deposit fines upslope above the height of the break in grain-size gradient within the suspension cloud;

10) Deposit aggraded during the unsteady phase fines upward as a result of grain-size decrease within the ponded cloud through time.

The described ponding flow behavior has implications for the structure of confined and ponded turbidite deposits, and it can help explain: a) single and multiple paleocurrent reversals within one single bed; b) weak normal grading throughout the entire bed thickness arising under steady input; c) repetitions of sedimentary structures (cyclicity), close to the confining slope; d) sharp breaks in grain-size gradient in the upper part of the bed; e) presence of unusually thick mud caps; f) thinning and fining upslope vs. abrupt pinch-out geometry.

ACKNOWLEDGMENTS

This research was funded by Turbidites Research Group sponsors Anadarko, BG-Group, BHP Billiton, BP, Chevron, ConocoPhillips, Kerr McGee, Devon, Maersk, Marathon, Nexen, Petronas, Shell, Statoil and Woodside. Gratitude goes to Gareth Keevil for his invaluable help in the laboratory. We thank

Associate Editor Stephen Hubbard and reviewers Julian Clark and Roberto Tinterri for their constructive comments, which helped improve an earlier version of this paper. We are indebted to Corresponding Editor John Southard for his careful editing of the final version of the manuscript.

REFERENCES CITED

Al Ja'Aidi, O.S., McCaffrey, W.D., and Kneller, B.C., 2004, Factors influencing the deposit geometry of experimental turbidity currents: implications for sand-body architecture in confined basins, *in* Lomas, S.A., and Joseph, P., eds., Confined Turbidite Systems: Geological Society of London, Special Publication 222, p. 45-58.

Alexander, J., and Morris, S., 1994, Observations on experimental, nonchannelized, high-concentration turbidity currents and variations in deposits around obstacles: Journal of Sedimentary Research, v. A64, p. 899-909.

Amy, L.A., McCaffrey W.D., and Kneller B.C., 2004, The influence of a lateral basin-slope on the depositional patterns of natural and experimental turbidity currents, *in* Joseph, P., and Lomas, S.A., eds., Deep-Water Sedimentation in the Alpine Basin of SE France: New perspectives on the Grès d'Annot and related systems: Geological Society of London, Special Publication 221, p. 311-330.

Apel, J.R., 2002, Oceanic Internal Waves and Solitons, *in* Jackson, C.R., and Apel, J.R., eds., An Atlas of Oceanic Internal Solitary Waves: Global Ocean Associates, 14605 Carrolton Rd., Rockville, MD 20853, United States, p. 1-40.

Baas, J.H., and De Koning, H., 1995, Washed-out ripples: their equilibrium dimensions, migration rate, and relation to suspended-sediment concentration in very fine sand: Journal of Sedimentary Research, v. A65, p. 431-435.

Baas, J.H., McCaffrey, W.D., Haughton, P.D.W., and Choux, C., 2005, Coupling between suspended sediment distribution and turbulence structure in a laboratory turbidity current: Journal of Geophysical Research, v. 110, no. C11015.

Bakke, K., Kane, I.A., Martinsen, O.J., Petersen, S.A., Johansen, T.A., Hustoft, S., Jacobsen, F.H., and Groth, A., 2013, Seismic modeling in the analysis of deep-water sandstone termination styles: American Association of Petroleum Geologists, Bulletin, v. 97, p. 1395-1419.

Baruffini, L., Cavalli, C., and Papani, L., 1994, Detailed stratal correlation and stacking patterns of the Gremiasco and lower Castagnola turbidite systems, Tertiary Piedmont Basin, northwestern Italy, *in* Weimer, P., Bouma, A. H. and Perkins, B. F., eds., Gulf Coast Section SEPM Foundation, 15th Annual Research Conference, Submarine Fans and Turbidite Systems: Sequence Stratigraphy, Reservoir Architecture and Production Characteristics, Gulf of Mexico and International, p. 9-21.

Best, J.L., Bennet, S., Bridge, J., and Leeder, M., 1997, Turbulence modulation and particle velocities over flat sand bends at low transport rates: Journal of Hydraulic Engineering, v. 123, p. 1118-1129.

Best, J.L., Kirkbride, A.D., and Peakall, J., 2001, Mean flow and turbulence structure of sediment-laden gravity currents: new insights using ultrasonic Doppler velocity profiling, *in* McCaffrey, W.D., Kneller, B.C., and Peakall, J., eds., Particulate Gravity Currents: International Association of Sedimentologists, Special Publication 31, p. 159-172.

Best, J.L., Kostaschuk, R.A., Peakall, J., Villard, P.V., and Franklin, M., 2005, Whole flow field dynamics and velocity pulsing within natural sediment-laden underflows: Geology, v. 33, p. 765-768.

Bouma, A.H., 1962, Sedimentology of Some Flysch Deposits; A Graphic Approach to Facies Interpretation: Amsterdam, Elsevier, 168 p.

Buckee, C., Kneller, B., and Peakall, J., 2001, Turbulence structure in steady, solute-driven gravity currents, *in* McCaffrey, W.D., Kneller, B.C., and Peakall, J., eds., Particulate Gravity Currents: International Association of Sedimentologists, Special Publication 31, p. 159-172.

Bursik, M.I. and Woods, A.W., 2000, The effects of topography on sedimentation from particle-laden turbulent density currents: Journal of Sedimentary Research, v. 70, p. 53-63.

Davis, C., Haughton, P.D.W., McCaffrey, W.D., Scott, E., Hogg, N., and Kitching, D., 2009, Character and distribution of hybrid sediment gravity flow deposits from the outer Forties Fan, Palaeocene Central North Sea, UKCS: Marine and Petroleum Geology, v. 26, p. 1919-1939.

Edwards, D.A., Leeder M.R., Best J.L., and Pantin, H.M., 1994, On experimental reflected density currents and the interpretation of certain turbidites: Sedimentology, v. 41, p. 437-461.

Elghobashi S., 1994, On predicting particle-laden turbulent flows: Applied Scientific Research, v. 52, p. 309-329.

Felletti, F., 2002, Complex bedding geometries and facies associations of the turbiditic fill of a confined basin in a transpressive setting (Castagnola Fm., Tertiary Piedmont Basin, NW Italy): Sedimentology, v. 49, p. 645-667.

Haughton, P.D.W., 1994, Deposits of deflected and ponded turbidity currents, Sorbas Basin, Southeast Spain: Journal of Sedimentary Research, v. A64, p. 233-246.

Haughton, P.D.W., 2000, Evolving turbidite systems on a deforming basin floor, Tabernas, SE Spain: Sedimentology, v 47, p. 497-518.

Haughton, P.D.W., Davis C., McCaffrey W., and Barker S., 2009, Hybrid sediment gravity flow deposits – Classification, origin and significance: Marine and Petroleum Geology, v. 26, p. 1900-1918.

Hetsroni, G., 1989, Particle-turbulence interaction: Journal of Multiphase Flow, v. 15, p. 735-746.

Holman, W.E., and Robertson, S.S., 1994, Field development, depositional model and production performance of the turbiditic "J" sands at prospect Bullwinkle, Green Canyon 65 fields, outer-shelf Gulf of Mexico, *in* Weimer, P., Bouma, A.H., and Perkins, B.F., eds., Submarine Fans and Turbidite Systems – Sequence Stratigraphy, Reservoir Architecture, and Production Characteristics: Gulf Coast Section SEPM, Fifteenth Annual Research Conference, p. 139-150.

Jobe, Z.R., Lowe, D.R., and Morris, W.R., 2012, Climbing-ripple successions in turbidite systems: depositional environments, sedimentation rates and accumulation times: Sedimentology, v. 59, p. 867-898.

Kneller, B.C., Edwards, D.A., McCaffrey, W.D., and Moore, R., 1991, Oblique reflection of turbidity currents: Geology, v. 19, p. 250-252.

Kneller, B.C., Bennet, S.J., and McCaffrey, W.D., 1997, Velocity and turbulence structure of density currents and internal solitary waves: potential sediment transport and the formation of wave ripples in deep water: Sedimentary Geology, v. 112, p. 235-250.

Kneller, B.C., and Buckee, C., 2000, The structure and fluid mechanics of turbidity currents: a review of some recent studies and their geological implications: Sedimentology, v. 47, Suppl. 1, p. 62-94.

Kneller, B., Edwards, D., McCaffrey, W., and Moore, R., 1991, Oblique reflection of turbidity currents: Geology, v. 14, p. 250-252.

Kneller, B., and McCaffrey, W., 1999, Depositional effects of flow nonuniformity and stratification within turbidity currents approaching a bounding slope deflection, reflection, and facies variation: Journal of Sedimentary Research, v. 69, p. 980-991.

Leeder, M.R., Gray, T.E., and Alexander, J., 2005, Sediment suspension dynamics and a new criterion for the maintenance of turbulent suspensions: Sedimentology, v. 52, p. 683-691.

Lamb, M.P., Hickson, T., Marr, J.G., Sheets, B., Paola, C., and Parker, G., 2004, Surging versus continuous turbidity currents flow dynamics and deposits in an experimental intraslope minibasins: Journal of Sedimentary Research, v. 74, p. 148-155.

Lowe, D.R., 1982, Sediment gravity flows: II. Depositional models with special reference to the deposits of high-density turbidity currents: Journal of Sedimentary Petrology, v. 52, p. 279-297.

Mahaffie, M.J., 1994, Reservoir classification for turbidite intervals at the Mars discovery, Mississippi Canyon 807, Gulf of Mexico, *in* Weimer, P., Bouma, A.H., and Perkins, B.F., eds., Submarine Fans and Turbidite Systems – Sequence Stratigraphy, Reservoir Architecture, and Production Characteristics: Gulf Coast Section SEPM, Fifteenth Annual Research Conference, p. 233-244.

McCaffrey, W.D. and Kneller, B.C., 2001, Process controls on the development of stratigraphic trap potential on the margins of confined turbidite systems and aids to reservoir evaluation: American Association of Petroleum Geologists, Bulletin, v. 85, p. 971-988.

Muck, M.T., and Underwood, M.B., 1990, Upslope flow of turbidity currents: A comparison among field observations, theory, and laboratory models: Geology, v. 18, p. 54-57.

Mutti, E., 1992, Turbidite Sandstones: San Donato Milanese, Agip-Istituto di Geologia, Università di Parma, Parma, 275 p.

Muzzi Magalhaes, P., and Tinterri, R., 2010, Stratigraphy and depositional setting of slurry and contained (reflected) beds in the Marnoso-arenacea Formation (Langhian-Serravallian) Northern Apennines, Italy: Sedimentology, v. 57, p. 1685-1720.

Owen, P.R., 1969, Pneumatic transport: Journal of Fluid Mechanics, v. 39, p. 407-432.

Pantin, H.M., and Leeder, M.R., 1987, Reverse flow in turbidity currents: the role of internal solitons: Sedimentology, v. 34, p. 1143-1155.

Patacci, M., Haughton, P.D.W., and McCaffrey, W.D., 2014, Rheological complexity in sediment gravity flows forced to decelerate against a confining slope, Braux, SE France: Journal of Sedimentary Research, v. 84, p. 270-277.

Pickering, K.T., and Hiscott, R.N., 1985, Contained (reflected) turbidity currents from the Middle Ordovician Cloridorme Formation, Quebec, Canada: an alternative to the antidune hypothesis: Sedimentology, v. 32, p. 373-394.

Remacha, E., Fernandez, L.P., and Maestro, E., 2005, The transition between sheet-like lobe and basin-plain turbidites in the Hecho basin (South-Central Pyrenees, Spain): Journal of Sedimentary Research, v. 75, p. 798-819.

Sequeiros, O.E., Spinewine, B., Garcia, M.H., Beaubouef, R.T., Sun, T., and Parker, G., 2009, Experiments on wedge-shaped deep sea sedimentary deposits in minibasins and/or on channel levees emplaced by turbidity currents. Part I. Documentation of the flow: Journal of Sedimentary Research, v. 79, p. 593-607.

Sinclair, H.D., 2000, Delta-fed turbidites infilling topographically complex basins: a new depositional model for the Annot Sandstones, SE France: Journal of Sedimentary Research, v. 70, p. 504-519.

Smith, R.U., 2004, Silled sub-basins to connected tortuous corridors: sediment distribution systems on topographically complex sub-aqueous slopes, *in* Lomas, S.A., and Joseph, P., eds., Confined Turbidite Systems: Geological Society of London, Special Publication 222, p. 23-43.

Takeda, Y., 1991, Development of an ultrasound velocity profile monitor: Nuclear Engineering and Design, v. 126, p. 277-284.

Tinterri, R., 2011, Combined flow sedimentary structures and the genetic link between sigmoidal- and hummocky-cross stratification: GeoActa (Bologna), v. 10, p. 1-43.

Tinterri, R., and Muzzi Magalhaes, P., 2011, Synsedimentary structural control on foredeep turbidites: An example from Miocene Marnoso-arenacea Formation, Northern Apennines, Italy: Marine and Petroleum Geology, v. 28, p. 629-657.

Toniolo, H., Lamb, M., And Parker, G., 2006a, Depositional turbidity currents in diapiric minibasins on the continental slope: formulation and theory: Journal of Sedimentary Research, v. 76, p. 783-797.

Toniolo, H., Parker, G., Voller, V., and Beaubouef, R.T., 2006b, Depositional turbidity currents in diapiric minibasins on the continental slope: experiments-numerical simulation and upscaling: Journal of Sedimentary Research, v. 76, p. 798-818.

Twichell, D.C., Cross, V.A., Hanson, A.D., Buck, B.J., Zybala, J.G., and Rudin, M.J., 2005, Seismic architecture and lithofacies of turbidites in lake Mead (Arizona and Nevada, U.S.A.), an analogue for topographically complex basins: Journal of Sedimentary Research, v. 75, p. 134-148.

Van Andel, T.H., and Komar, P.D., 1969, Ponded sediments of the Mid-Atlantic Ridge between 22° and 23° north latitude: Geological Society of America, Bulletin, v. 80, p. 1163-1190.

Winker, C.D., 1996, High-resolution seismic stratigraphy of a Late Pleistocene submarine fan ponded by salt-withdrawal mini-basins on the Gulf of Mexico continental slope, *in* Offshore Technology Conference, paper 8024, p. 619-628.

TABLE AND FIGURE CAPTIONS

Table 1. Main set-up characteristics and input conditions of the described experimental runs.

Figure 1. Different types of interaction between turbidity currents and topography depend on the geometry of the slope and the angle of incidence of the current. If the scale of the topography is similar or greater than the flow, A) deflection (flow reorientation), B) reflection (flow direction reversed), or C) constriction (current has to pass through a narrow slot) can occur. When the flow

(either surge-like or sustained) is partially or fully contained by topography, flow ponding (D) takes place.

Figure 2. Examples of confined and ponded turbidites. A) Sandstone bed showing opposing palaeocurrent directions (arrows) from the Cloridorme Fm., Canada (from Pickering and Hiscott, 1985. B) Turbidite bed showing vertical repetition of couplets of cross-laminated sandstone (xl) and massive sandstone (m) (from Felletti, 2002). C) Log of typical contained bed from the Sorbas Basin (from Haughton, 1994). D) Sandstone bed with multiple palaeocurrent directions and a thick mudstone cap (from Muzzi Magalhaes and Tinterri, 2010). E) Bed with unusual vertical sequence of sedimentary structures (Bouma divisions Tb-Tc-Ta) from the Tabernas Basin (from Haughton, 2000).

Figure 3. A, B) Geometry of experimental tanks. Measuring localities indicate location of velocity and concentration profiles. Profiles were measured orthogonal to the floor, irrespective of whether this was flat or sloping. The water level was kept constant during runs using an outlet pump located at the lower part of the downstream end of the main flume. C) Grain-size distribution for Vaquashene batch used for experiment L1 (pilot experiment). D_{50} is 39 µm. Measured with Malvern Mastersizer 2000 (average of 30 samples). D) UVP geometry was designed to allow non-intrusive measure of 3D velocity. Measuring axes are shown as dotted lines.

Figure 4. A, B, C) Combined data and interpretations from runs L4 and L5 showing the evolution of the first velocity reversal and bore migration. D) Data and interpretation from run L6, pointing out the internal structure of a ponded turbidity current. Video frames are plotted onto the tank drawing. Flow geometry is highlighted (dirty water is highlighted in light gray). Small arrows indicate measured 3D velocity plotted on the view plane (parallel to side walls of the experimental tank). Length of the vectors indicates intensity of the field. Large arrows show interpreted flow structure.

Figure 5. Time-height plots of 3D velocity. Arrows represent 3D velocity plotted on a plane parallel to side walls. Colors show streamwise velocity (hot colors: outbound flow; cold colors: return flow). A,

B) First velocity reversal (see text for explanation) on the slope (65 to 85 seconds after begin of pumping) and in the flat part of the basin (90 to 100 seconds). C, D) Basal outbound layer of a ponded turbidity current in the basin floor and on the slope respectively. E) Basal outbound layer and the upper return layer within a ponded turbidity current at the slope location. Internal velocity interface is highlighted. Note that the measuring range is able to cover most of the thickness of the flow in comparison to Parts C and D.

Figure 6. Time series for experiments L3, L4, and L5 measured 12.5 cm above the floor. Velocity values are plotted at 1 Hz. Moving average (30 s window) is shown (thick line with open circles) for vertical velocity (independent axis on the right) and streamwise velocity. 3D RMS velocity plots include 2.4 cm space window 3D RMS (thick line) and 5 s time window 3D RMS (thin line). 3D RMS velocities are calculated averaging the three spatial components (for time window) or adding 2/3 of the horizontal component to 1/3 of the vertical component (for space window).

Figure 7. Characteristic vertical profiles for Ga (left) and L6 (right). Streamwise velocity and concentration are shown. Points represent measured values. Gray color shows the thickness of the sediment bearing cloud. A curve of relative grain size (absolute values not indicated) is added to the Ga plot to highlight the similar geometrical distribution of the gradients of concentration and grain size.

Figure 8. A, B) Frames from video recordings (run L4) are shown after conversion to b/w as part of the image-analysis processing to extract internal-waves time series. In each frame, the gray box indicates the observation window, and the upper boundary of the black subhorizontal band can be used as a proxy for the position of the upper surface of the ponded interface. The two frames (10 seconds apart) show A) the trough and B) the crest of the same wave displacing the ponded interface above the confining slope. C) Time series of the amplitude of internal waves measured using image analysis of video recordings. D) Velocity structure of internal waves (UVP data). Black arrows represent 3D velocity vectors plotted on a plane parallel to the side walls. Thick gray arrows

highlight orbital motion and position of the internal waves. E) Average amplitude of internal waves (normalized to flow thickness) is plotted against average dominant frequency. Experimental runs cluster according to the type of internal concentration interface in the ponded suspension.

Figure 9. Basal flow reversals. Time-height color plots of streamwise velocity are used to illustrate the three types of flow reversals that characterize the basal layer of the ponded suspension. Note that the first flow reversal (type A) can comprise a single reversal event (as shown here) or a small number of them (e.g., see Fig. 5A).

Figure 10. Evolution of the average concentration of the ponded cloud calculated for a layer between 2.5 and 22.5 cm above the confining slope. Four runs are shown: full diamond (L5, 2l/s and 10 deg slope), full triangle (L6, 1 l/s and 10 deg slope), empty diamond (L8, 2 l/s and 10 deg slope) and empty triangle (L9, 1 l/s and 15 deg slope). Continuous lines are exponential best-fitting equations ($R^2 > 0.995$). Concentration increases during the 600 seconds of pumping time, but the increase becomes smaller through time: this is characteristic of the unsteady ponded phase and records the progressive approaching to the steady phase.

Figure 11. Evolution of the sediment grain size in the ponded suspension (run L5). Data are sampled between 2.5 and 22.5 cm above the slope, all falling within the basal ungraded layer. Each value is measured from a fluid sample which represents an average over 8 seconds. The data scatter (~ 1 µm) is mostly due to temporal and spatial nonuniform grain-size distribution, as methodology error is smaller. Black line represents the average value for the entire layer.

Figure 12. Average deposit grain size in the basin (left) toward the lip of the confining slope (right). Each point represents the average of three repeated measurements on one deposit sample (laser grain sizer). Dashed lines are interpretations.

Figure 13. Vertical grain-size trends in the deposit from run Gb were measured using SEM images of fixed deposit (left). Bin size (for average): 1 mm; bin overlap: 75%. Note that two lines are plotted for

samples B and C (adjacent measures). Deposit on the slope is finer than that on the basin floor. Sample B shows weak upward fining until the gray arrow (sediment deposited during the unsteady phase from the lower part of the ponded cloud), then a very sharp upward fining (sediment deposited, after pump is switched off, from the upper part of the cloud). Sample C has a similar pattern, but the upward fining of the basal part of the deposit is stronger. Note that the value shown is the apparent grain diameter (neither the actual real grain diameter nor the D_{50}) and absolute comparison with laser particle sizer data could not be achieved.

Figure 14. Summary of the key flow features of a ponded suspension cloud resulting from the partial or the full trapping of a fully turbulent, low density and sustained turbidity current.

name	**confinement**	**basin size (w x l)** *cm*	**inlet slope**	**discharge type**	**inlet system**	**discharge duration** *s*	**discharge start-end** *l/s*	**concentration start-end** *%vol*
Ga	2 slopes & wall	35 x 300	no	double pipe	pump	600	2.3-2.1	(3%)
Gb	2 slopes & wall	35 x 300	no	double pipe	pump	600	1.5-1.3	(3%)
Gc	2 slopes & wall	35 x 300	no	double pipe	pump	600	2.0-1.7	(3%)
L3	unconfined	35 x unc.	10º	pipe	head tank	600	1.9	3.0-2.8
L4	10º slope	35 x 512	10º	pipe	head tank	600	1.9	3.0-2.8
L5	10º slope	35 x 512	10º	pipe	head tank	600	1.9	3.0-2.8
L6	10º slope	35 x 512	10º	pipe	head tank	600	1.0	2.7-2.5
L7	10º slope	35 x 512	10º	pipe	head tank	600	0.3	2.6-2.5
L8	15º slope	35 x 520	10º	pipe	head tank	600	1.9	2.8-2.5
L9	15º slope	35 x 520	10º	pipe	head tank	600	1.0	2.5-2.3

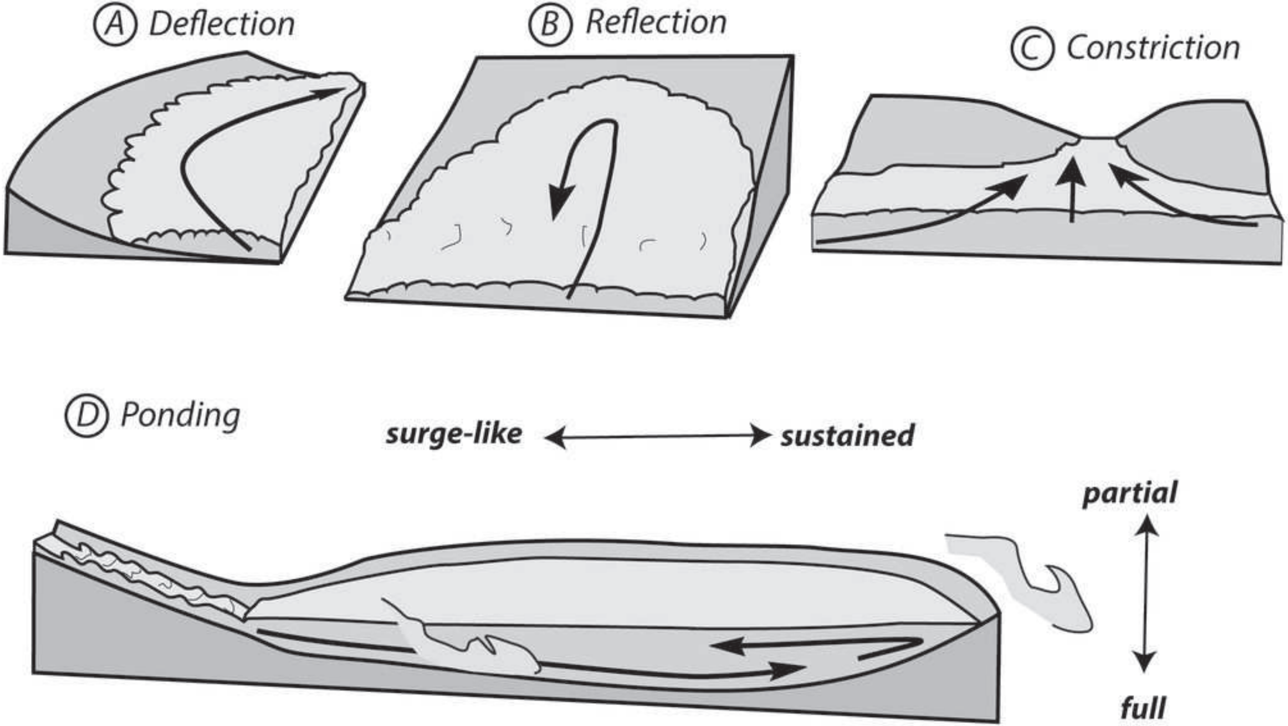

A Deflection
B Reflection
C Constriction
D Ponding
surge-like
sustained
partial
full

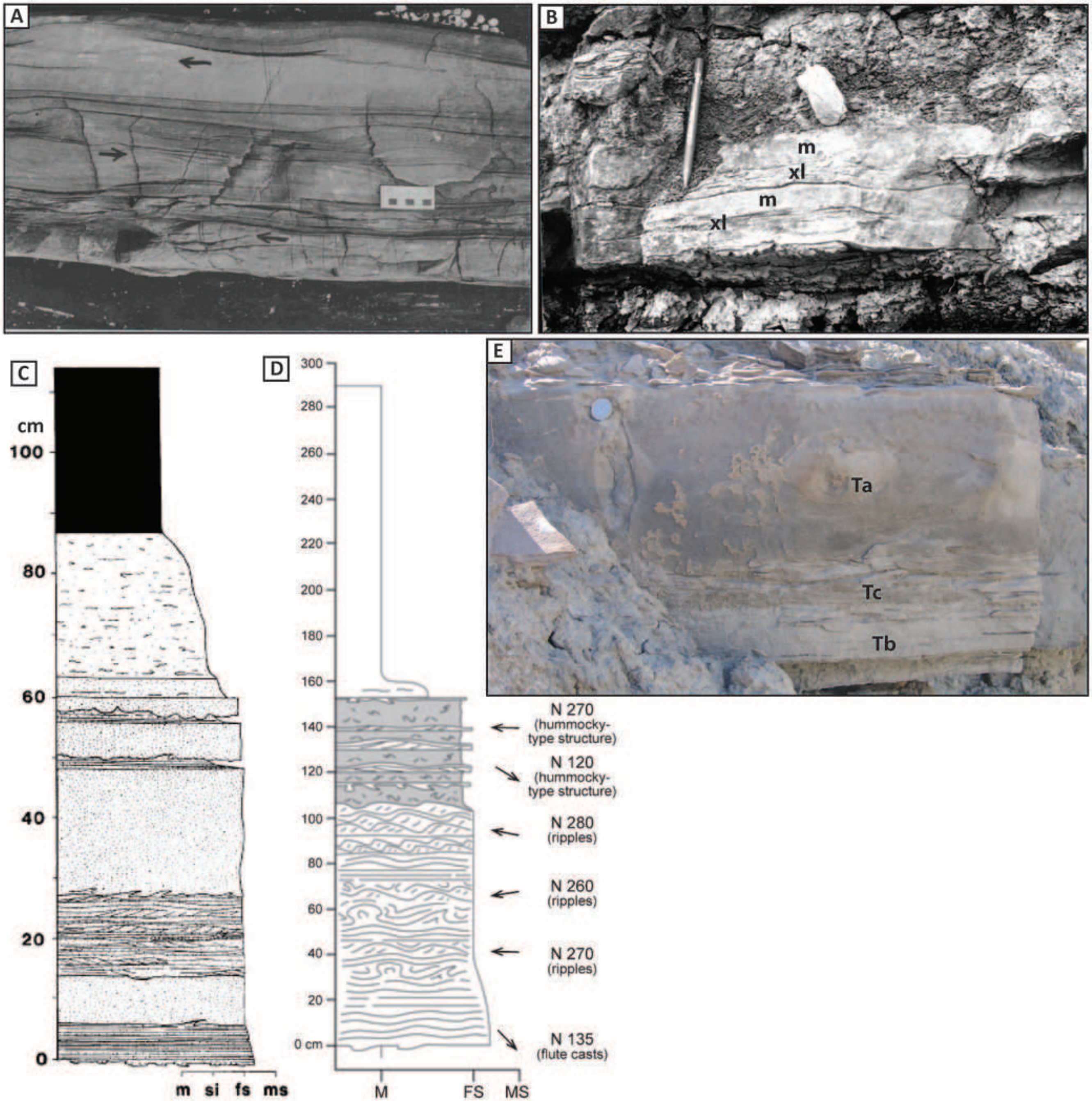
A
B
m
xl
m
xl
C
cm
100
80
60
40
20
0
m si fs ms
D
300
280
260
240
220
200
180
160
140
120
100
80
60
40
20
0 cm
M FS MS
N 270 (hummocky-type structure)
N 120 (hummocky-type structure)
N 280 (ripples)
N 260 (ripples)
N 270 (ripples)
N 135 (flute casts)
E
Ta
Tc
Tb

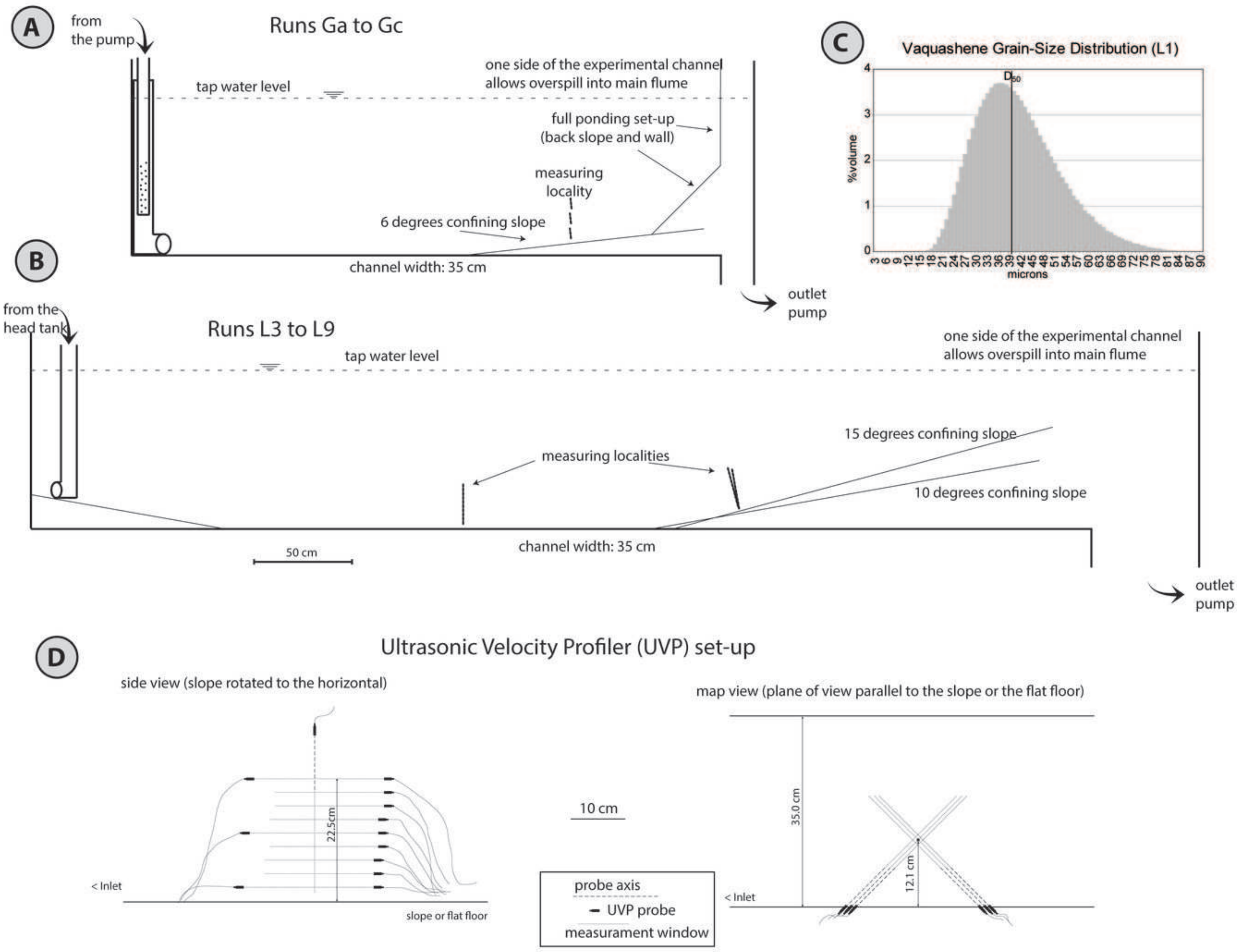

A
from
the pump
Runs Ga to Gc
tap water level
one side of the experimental channel
allows overspill into main flume
full ponding set-up
(back slope and wall)
measuring
locality
6 degrees confining slope
channel width: 35 cm
outlet
pump
C
Vaquashene Grain-Size Distribution (L1)
%volume
microns
D50
B
from the
head tank
Runs L3 to L9
tap water level
one side of the experimental channel
allows overspill into main flume
15 degrees confining slope
measuring localities
10 degrees confining slope
50 cm
channel width: 35 cm
outlet
pump
D
Ultrasonic Velocity Profiler (UVP) set-up
side view (slope rotated to the horizontal)
map view (plane of view parallel to the slope or the flat floor)
22.5cm
< Inlet
slope or flat floor
10 cm
probe axis
UVP probe
measurement window
35.0 cm
12.1 cm
< Inlet

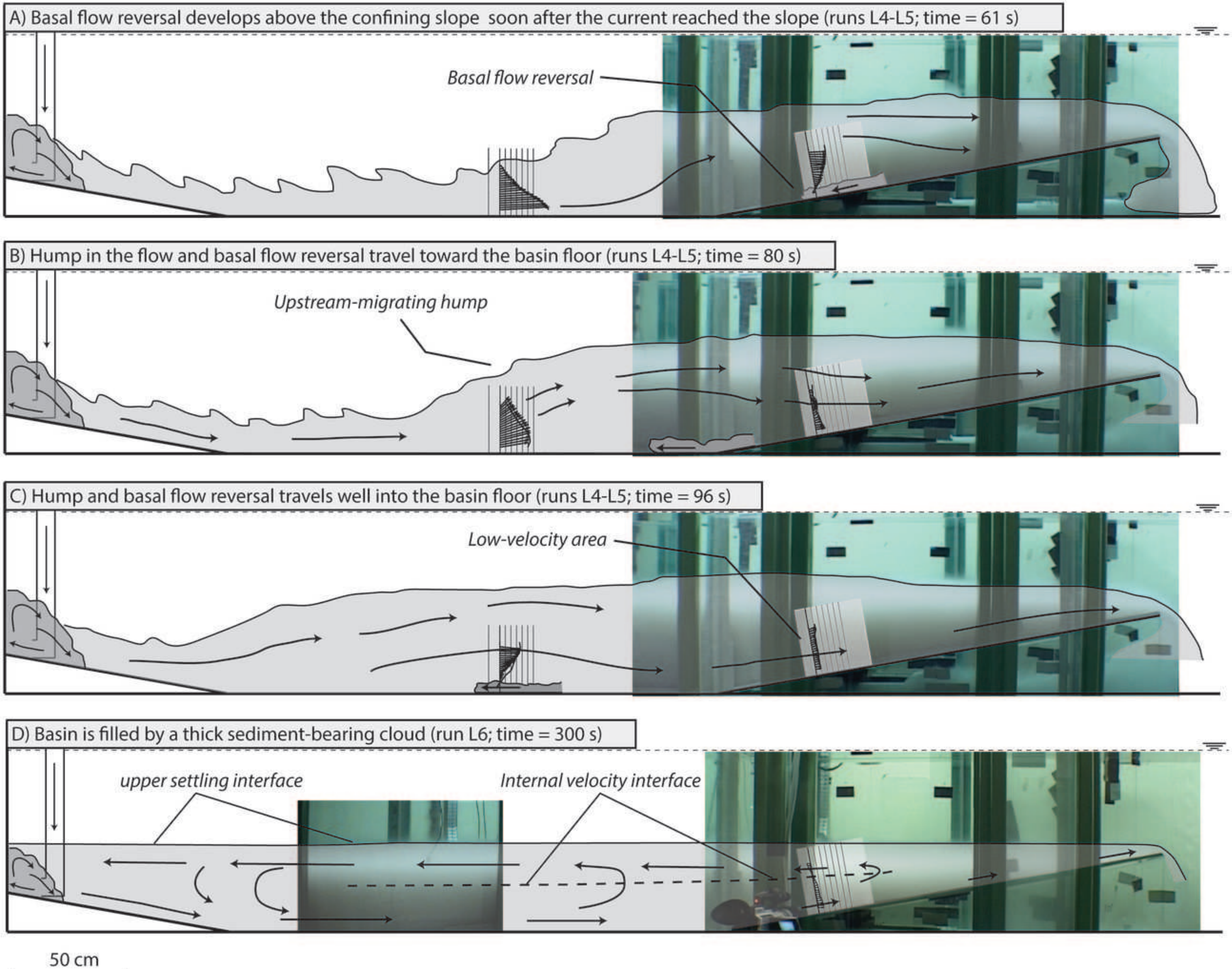
A) Basal flow reversal develops above the confining slope soon after the current reached the slope (runs L4-L5; time = 61 s)
Basal flow reversal
B) Hump in the flow and basal flow reversal travel toward the basin floor (runs L4-L5; time = 80 s)
Upstream-migrating hump
C) Hump and basal flow reversal travels well into the basin floor (runs L4-L5; time = 96 s)
Low-velocity area
D) Basin is filled by a thick sediment-bearing cloud (run L6; time = 300 s)
upper settling interface
Internal velocity interface
50 cm

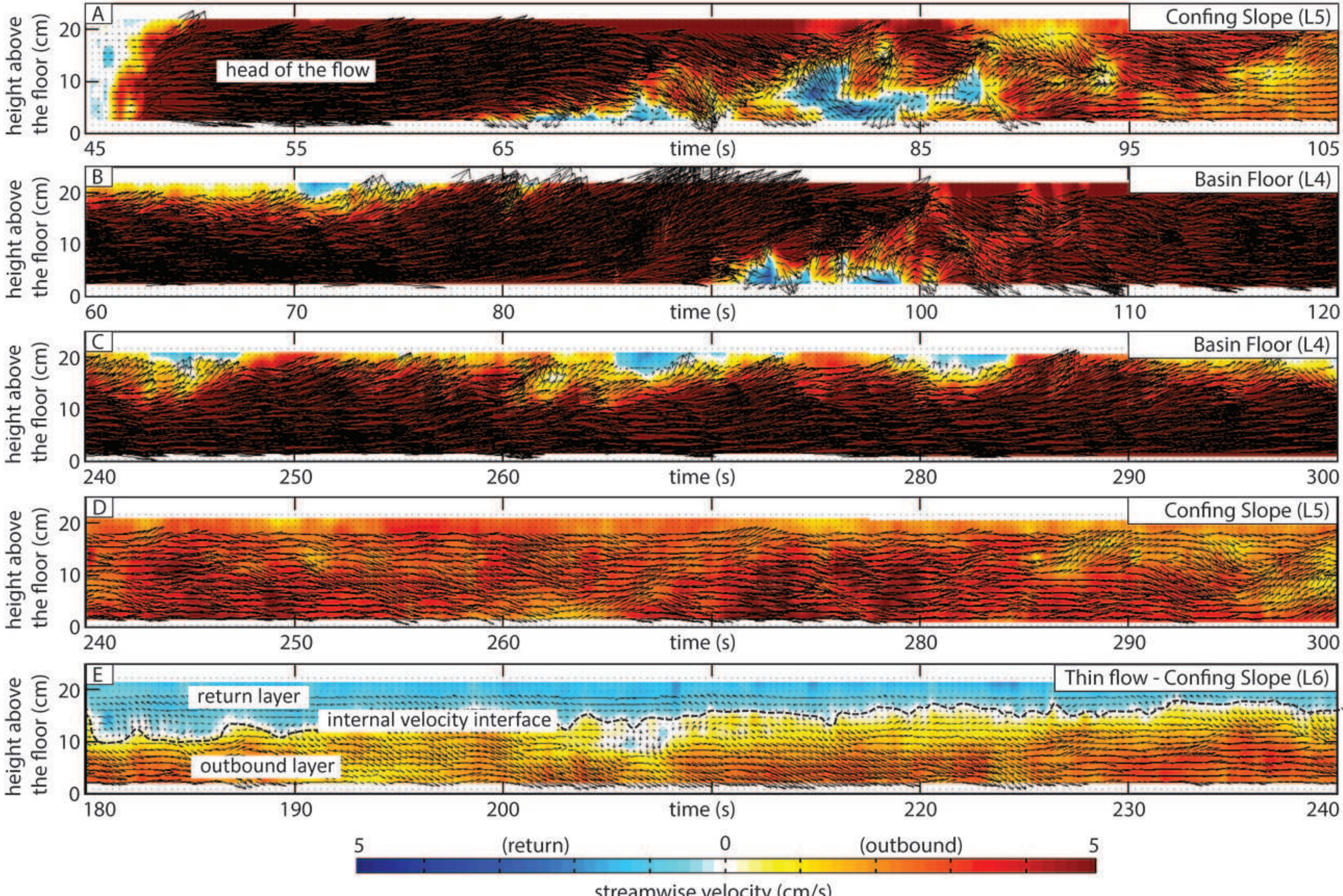

A
Confing Slope (L5)
head of the flow
height above the floor (cm)
time (s)
B
Basin Floor (L4)
C
Basin Floor (L4)
D
Confing Slope (L5)
E
Thin flow - Confing Slope (L6)
return layer
internal velocity interface
outbound layer
5
(return)
0
(outbound)
5
streamwise velocity (cm/s)

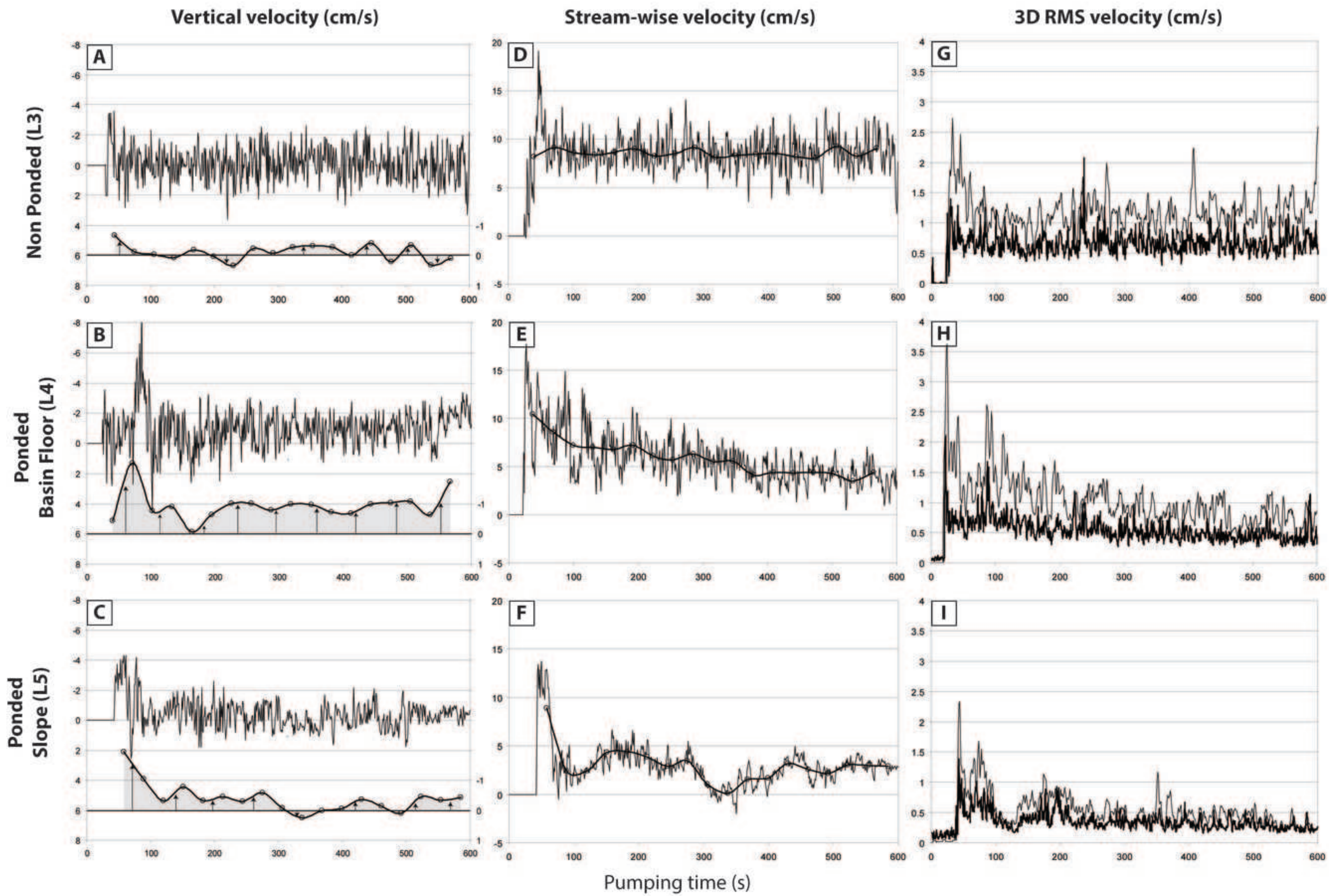

Vertical velocity (cm/s)
Stream-wise velocity (cm/s)
3D RMS velocity (cm/s)
Non Ponded (L3)
Ponded
Basin Floor (L4)
Ponded
Slope (L5)
A
B
C
D
E
F
G
H
I
Pumping time (s)

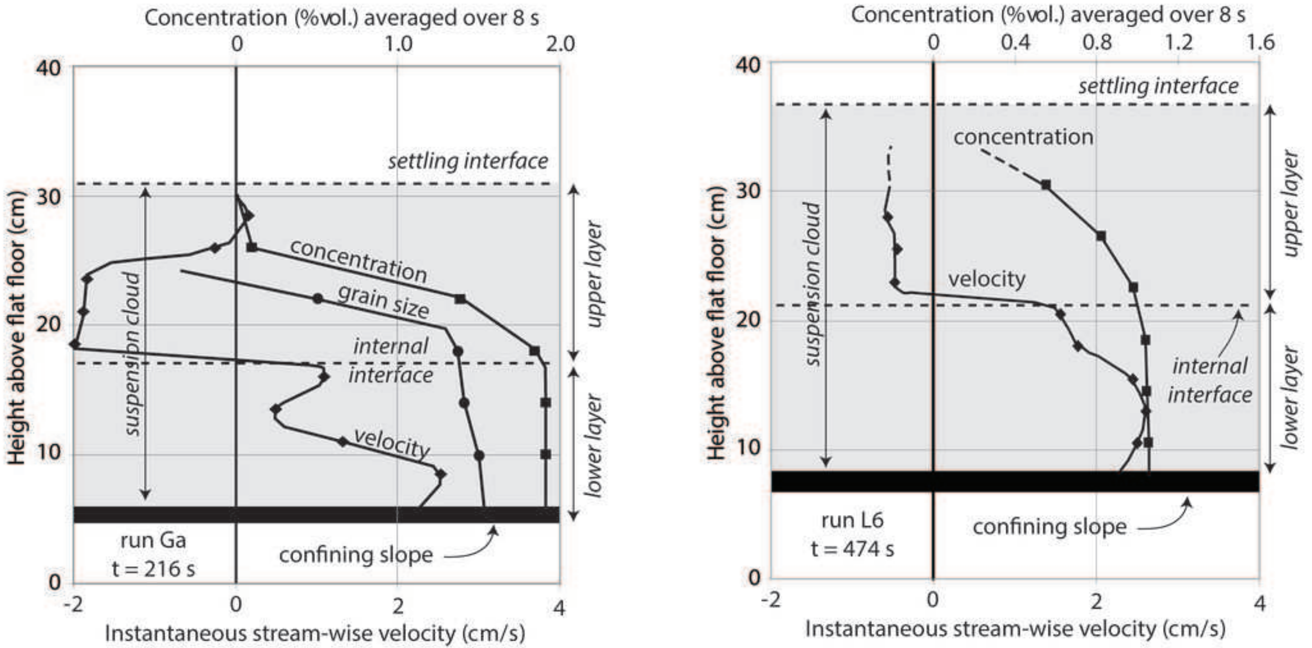

Concentration (%vol.) averaged over 8 s
0
1.0
2.0
40
30
20
10
0
Height above flat floor (cm)
settling interface
concentration
grain size
internal
interface
velocity
suspension cloud
upper layer
lower layer
run Ga
t = 216 s
confining slope
-2
0
2
4
Instantaneous stream-wise velocity (cm/s)
Concentration (%vol.) averaged over 8 s
0
0.4
0.8
1.2
1.6
40
30
20
10
0
Height above flat floor (cm)
settling interface
concentration
velocity
suspension cloud
upper layer
lower layer
internal
interface
run L6
t = 474 s
confining slope
-2
0
2
4
Instantaneous stream-wise velocity (cm/s)

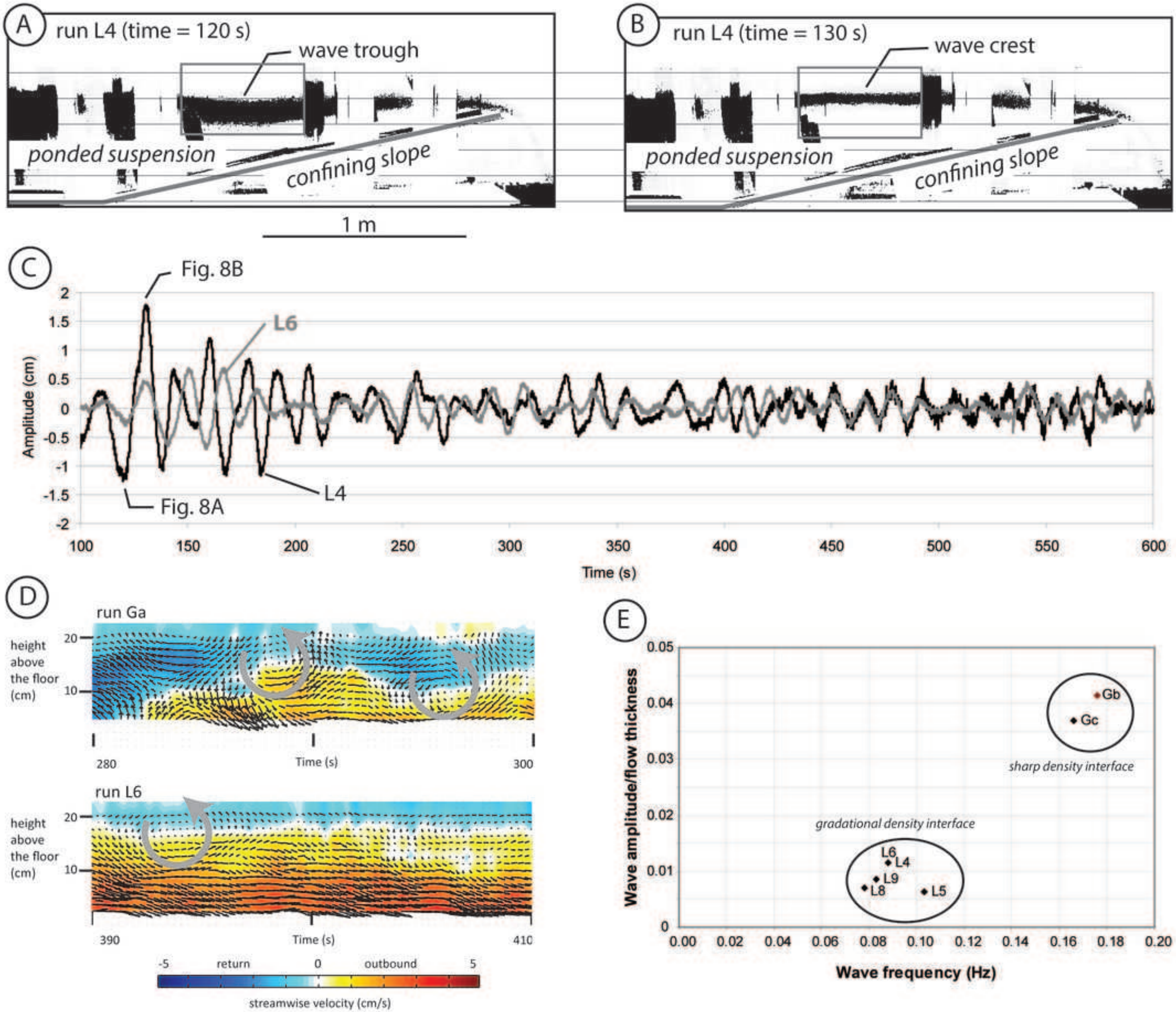
A
run L4 (time = 120 s)
wave trough
ponded suspension
confining slope
1 m
B
run L4 (time = 130 s)
wave crest
ponded suspension
confining slope
C
Fig. 8B
L6
Fig. 8A
L4
Amplitude (cm)
Time (s)
D
run Ga
height above the floor (cm)
280
Time (s)
300
run L6
390
410
-5 return 0 outbound 5
streamwise velocity (cm/s)
E
Wave amplitude/flow thickness
Wave frequency (Hz)
Gb
Gc
sharp density interface
gradational density interface
L6
L4
L9
L8
L5

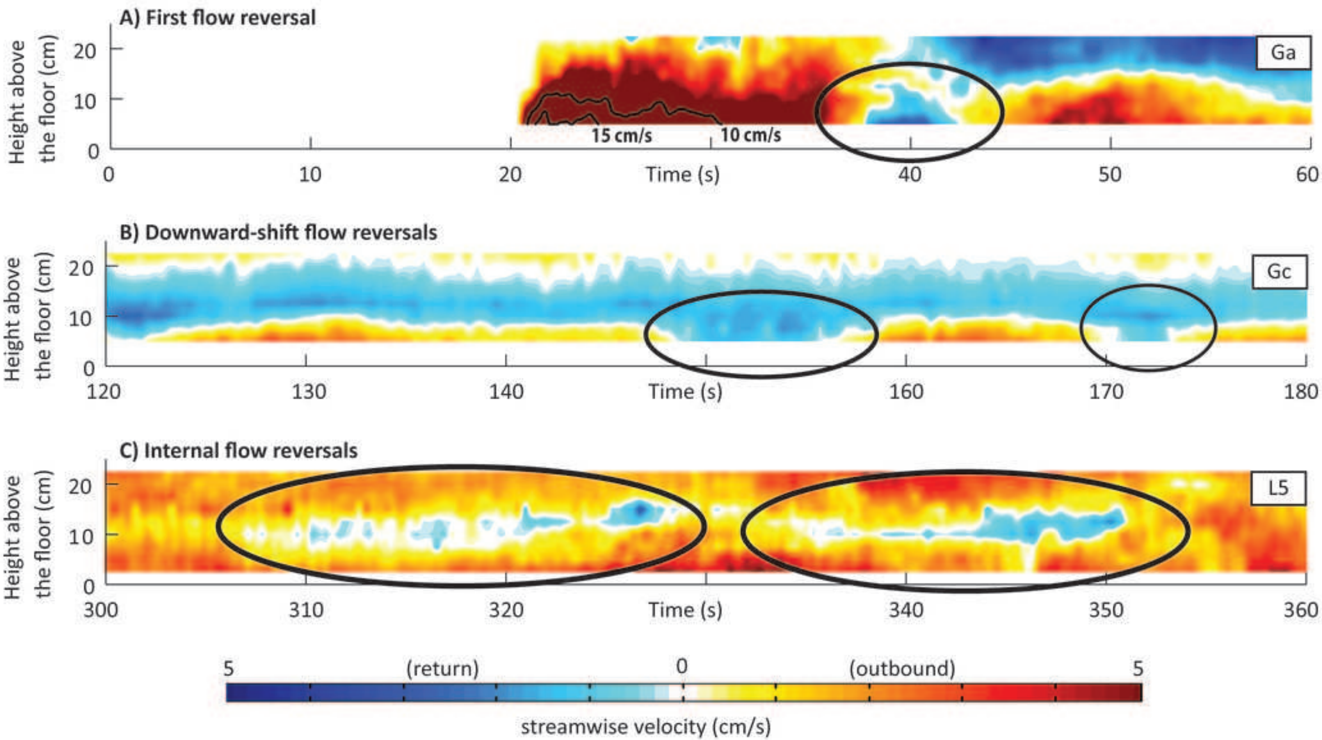
A) First flow reversal
Height above the floor (cm)
0
10
20
Ga
15 cm/s
10 cm/s
Time (s)
0
10
20
40
50
60
B) Downward-shift flow reversals
Height above the floor (cm)
0
10
20
Gc
Time (s)
120
130
140
160
170
180
C) Internal flow reversals
Height above the floor (cm)
0
10
20
L5
Time (s)
300
310
320
340
350
360
5
(return)
0
(outbound)
5
streamwise velocity (cm/s)

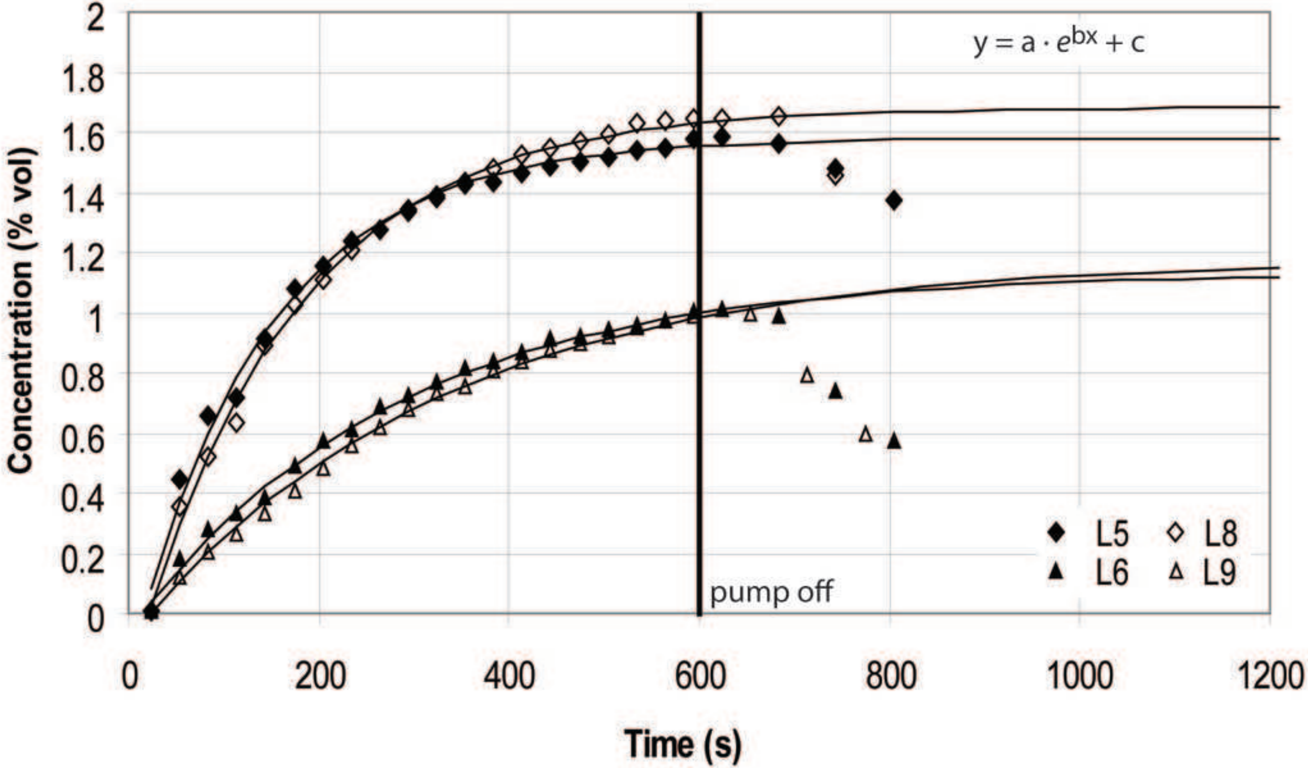

y = a · e^bx + c
Concentration (% vol)
Time (s)
pump off
L5
L8
L6
L9
0
0.2
0.4
0.6
0.8
1
1.2
1.4
1.6
1.8
2
0
200
400
600
800
1000
1200

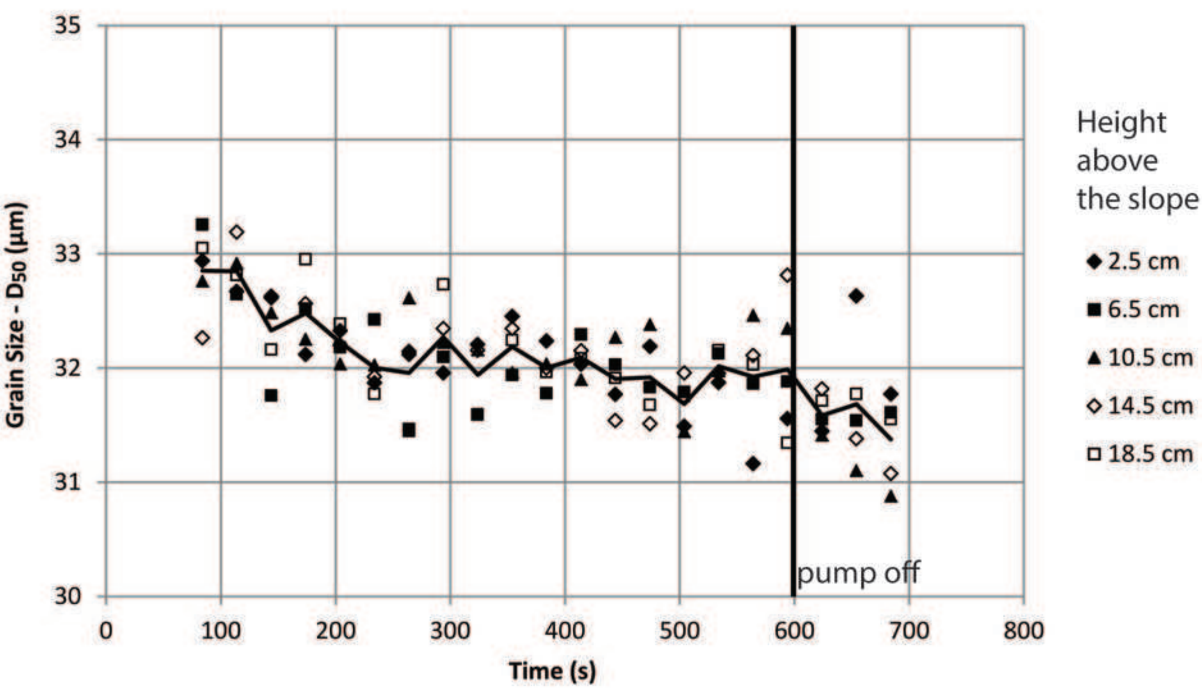

Grain Size - D_{50} (µm)
Time (s)
pump off
Height above the slope
2.5 cm
6.5 cm
10.5 cm
14.5 cm
18.5 cm
35
34
33
32
31
30
0
100
200
300
400
500
600
700
800

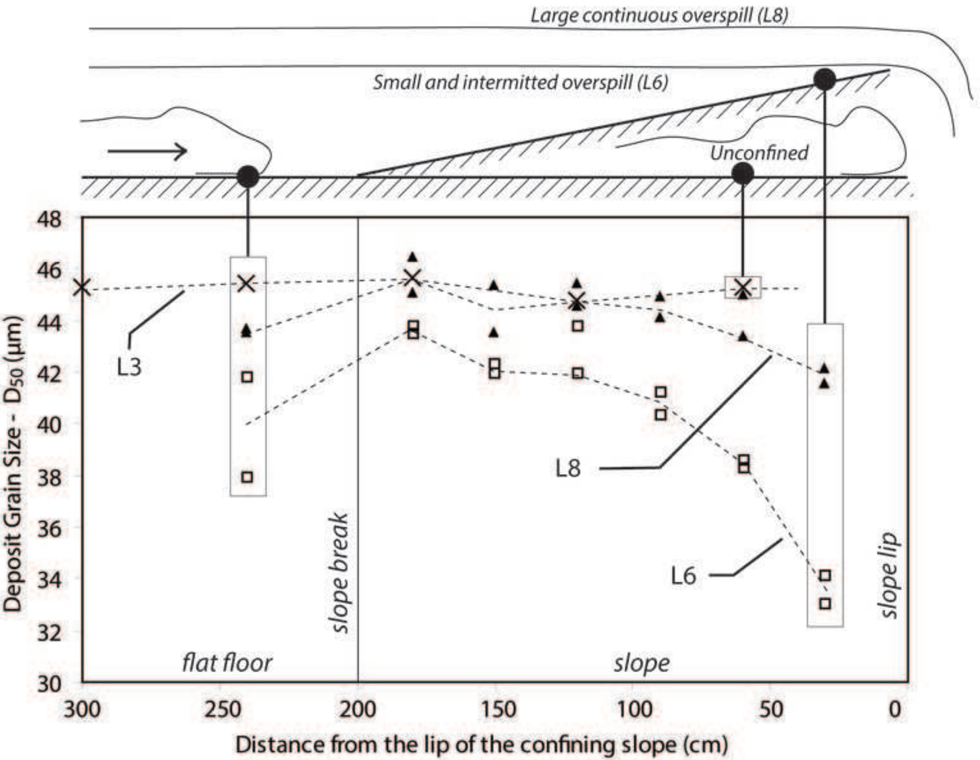
Large continuous overspill (L8)
Small and intermitted overspill (L6)
Unconfined
L3
L8
L6
slope break
slope lip
flat floor
slope
Deposit Grain Size - D50 (µm)
48
46
44
42
40
38
36
34
32
30
300
250
200
150
100
50
0
Distance from the lip of the confining slope (cm)

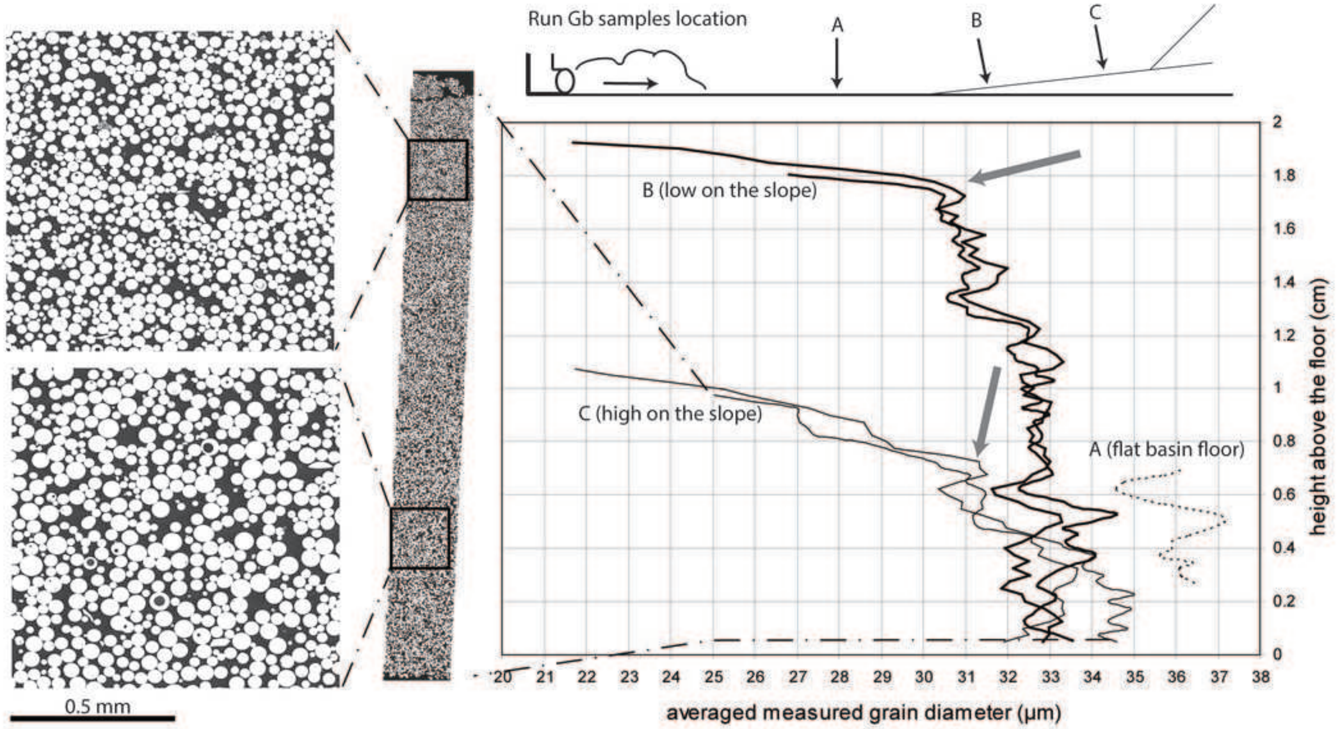

Run Gb samples location
A
B
C
B (low on the slope)
C (high on the slope)
A (flat basin floor)
height above the floor (cm)
0
0.2
0.4
0.6
0.8
1
1.2
1.4
1.6
1.8
2
20 21 22 23 24 25 26 27 28 29 30 31 32 33 34 35 36 37 38
averaged measured grain diameter (µm)
0.5 mm

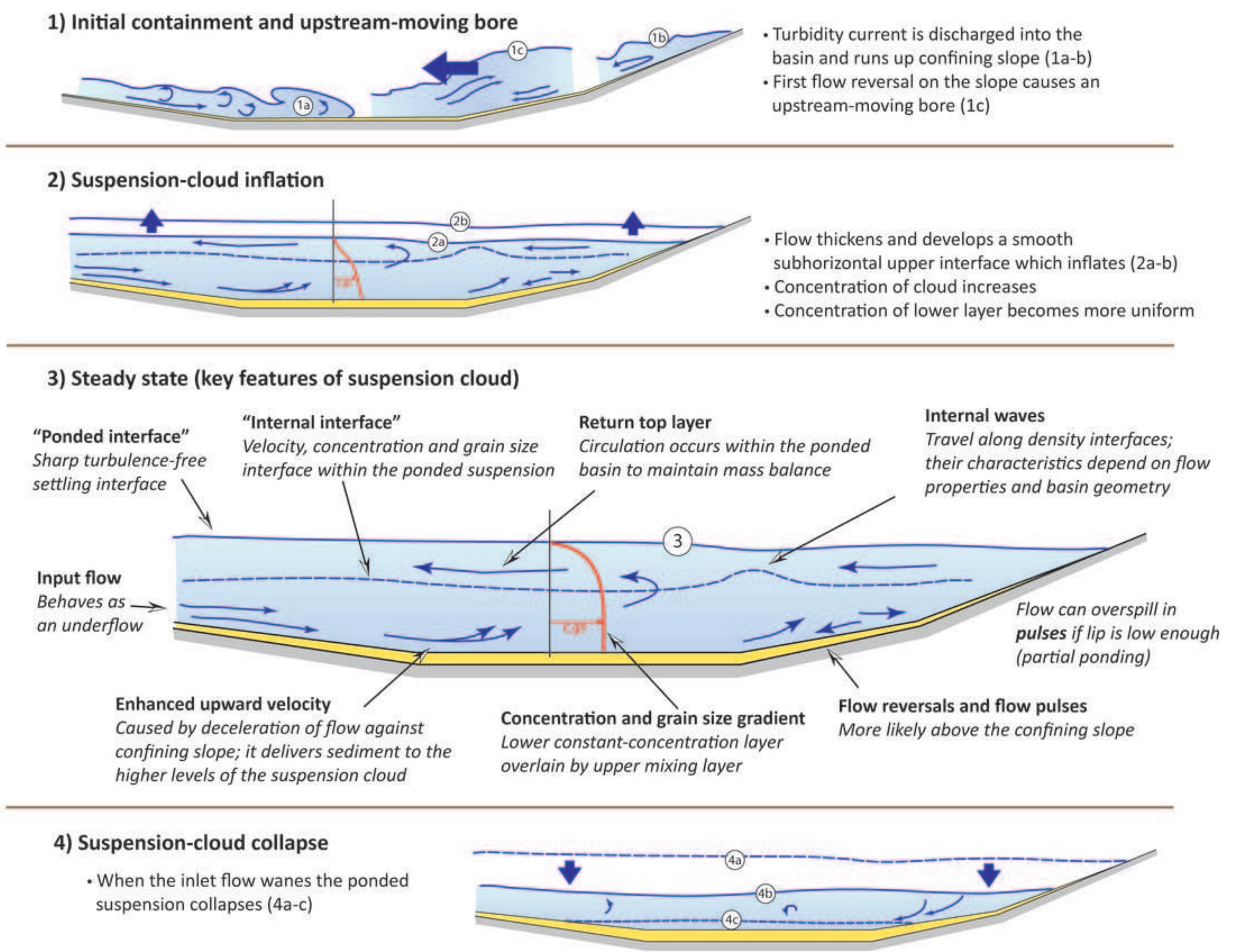
1) Initial containment and upstream-moving bore
1a
1b
1c
• Turbidity current is discharged into the basin and runs up confining slope (1a-b)
• First flow reversal on the slope causes an upstream-moving bore (1c)
2) Suspension-cloud inflation
2a
2b
• Flow thickens and develops a smooth subhorizontal upper interface which inflates (2a-b)
• Concentration of cloud increases
• Concentration of lower layer becomes more uniform
3) Steady state (key features of suspension cloud)
"Ponded interface"
Sharp turbulence-free settling interface
"Internal interface"
Velocity, concentration and grain size interface within the ponded suspension
Return top layer
Circulation occurs within the ponded basin to maintain mass balance
Internal waves
Travel along density interfaces; their characteristics depend on flow properties and basin geometry
3
Input flow
Behaves as an underflow
Flow can overspill in pulses if lip is low enough (partial ponding)
Enhanced upward velocity
Caused by deceleration of flow against confining slope; it delivers sediment to the higher levels of the suspension cloud
Concentration and grain size gradient
Lower constant-concentration layer overlain by upper mixing layer
Flow reversals and flow pulses
More likely above the confining slope
4) Suspension-cloud collapse
• When the inlet flow wanes the ponded suspension collapses (4a-c)
4a
4b
4c